How Stiff Was Armorica During the Variscan Orogeny? A Reappraisal of the "Bretonian" Phase in Central Brittany

Michel Faure, Eric Marcoux, Marc Poujol, Clément Masson

geosciences

MDPI

Article

How Stiff Was Armorica During the Variscan Orogeny? A Reappraisal of the "Bretonian" Phase in Central Brittany

Michel Faure [1,*], Eric Marcoux [1], Marc Poujol [2] and Clément Masson [1]

[1] Institut des Sciences de la Terre d'Orléans (ISTO), UMR 7327-CNRS/Université d'Orléans/BRGM, Campus Géosciences, 1A Rue de la Férollerie, F-45071 Orléans CEDEX 2, France; eric.marcoux55@gmail.com (E.M.)
[2] University Rennes, CNRS, Géosciences Rennes, UMR 6118, F-35000 Rennes, France; marc.poujol@univ-rennes.fr
* Correspondence: michel.faure@univ-orleans.fr

Abstract: In collision belts, the upper plate is generally less deformed than the lower one that underwent syn-metamorphic ductile shearing, and frequently late-collisional crustal melting. Concerning the Variscan orogeny, it is widely accepted that the Armorica microcontinent represented the upper plate of the collision system. In France, the Central-North-Armorican Domain belonged to this upper plate whose southern margin in the Pontivy–Coray area exposes metamorphic rocks. There, structural and metamorphic studies indicate that an early tectono-metamorphic event (M0-M1) with biotite–garnet–staurolite–kyanite assemblage, crystallized at 0.9 GPa and 500 °C, is characterized by a top-to-the NW shearing. This event was followed by an HT event (M2) at ca 800–900 °C, coeval with a domal structure. In micaschists, monazite yields an LA-ICP-MS age at 351 Ma ascribed to M2. M0-M1-M2 events developed before the Late Carboniferous pluton emplacement at ca 315 Ma (M3 event). The tectono-metamorphic succession documents that Armorica was not a rigid block but underwent a synmetamortphic ductile deformation during the Famennian–Tournaisian (360–355 Ma) collision redefined here as the late episode of the "Bretonian orogenic phase", whereas the pre-Famennian Bretonnian episode is ascribed to oceanic subduction. These new data allow us to reassess the geodynamic evolution of this part of the Variscan orogen.

Keywords: Variscan orogeny; Armorica microcontinent; Saxo-Thuringia; MP/MT metamorphism; monazite dating; Famennian–Tournaisian Bretonian phase

Academic Editor: Haakon Fossen

Received: 14 January 2025
Revised: 3 February 2025
Accepted: 5 February 2025
Published: 10 February 2025

Citation: Faure, M.; Marcoux, E.; Poujol, M.; Masson, C. How Stiff Was Armorica During the Variscan Orogeny? A Reappraisal of the "Bretonian" Phase in Central Brittany. *Geosciences* **2025**, *15*, 60. https://doi.org/10.3390/geosciences15020060

1. Introduction

In addition to the thermal gradient, the diversity of the tectonic styles in collision belts is also due to the lithological variety and the structural inheritance of the materials involved in the orogenic processes. For instance, in the Himalayas, the crustal thickening was accommodated in the lower plate by the tectonic stacking of metasedimentary series bounded by low-angle km scale ductile shear zones such as the Main Boundary Thrust, Main Central Thrust, Kangmar Thrust. These ductile thrusts developed within a thick pile of sedimentary rocks devoid of the older basement of the Indian lower plate, but in the Tibetan upper plate, the collision-related deformation is represented by less developed N-directed back thrusts, e.g., [1–7] and enclosed references. On the contrary, in the Alps, Cenozoic thrust sheets involve both a sedimentary cover and a gneissic basement deformed during the Variscan orogeny, e.g., [8–13]. It is now well acknowledged that the Variscan orogen results from multiple collisions between two large continents, namely Laurussia

and Gondwana, to the North and South, respectively, e.g., [14–24]; Figure 1. Moreover, intervening microcontinents such as Armorica and Saxo-Thuringia recognized at least from Iberia to Bohemia, and probably also in the Alpine basement, were involved in the orogenic events, e.g., [25–27], and enclosed references, Figure 1. It is also acknowledged that in the Early Ordovician, the microcontinents drifted from the North Gondwana margin, from which they were separated by oceanic domains. The existence of the Armorica block has long been suggested by paleogeographic reconstructions [28,29] and by paleomagnetism [30,31]. Due to limited geological constraints, the reality of the existence of the Armorica microplate was questioned (see extensive review in [32]). The similarity in faunal distribution of the Early Paleozoic assemblages between Armorica and Gondwana suggests that the oceanic domain was limited in size. Thus, a Red Sea-type ocean might account for the observed biogeographic features. In the following, we shall focus on the part of the Armorica block exposed in the Armorican Massif. There, the presence of mafic-ultramafic rocks, interpreted as ophiolites, along the Nort-sur-Erdre fault (North of Nantes) or in the Baie d'Audierne (Figure 2) supports the reality of an oceanic domain called the Medio-European ocean [17] or Galicia-Massif Central [14,15] that separated the Armorica block from the North Gondwana margin.

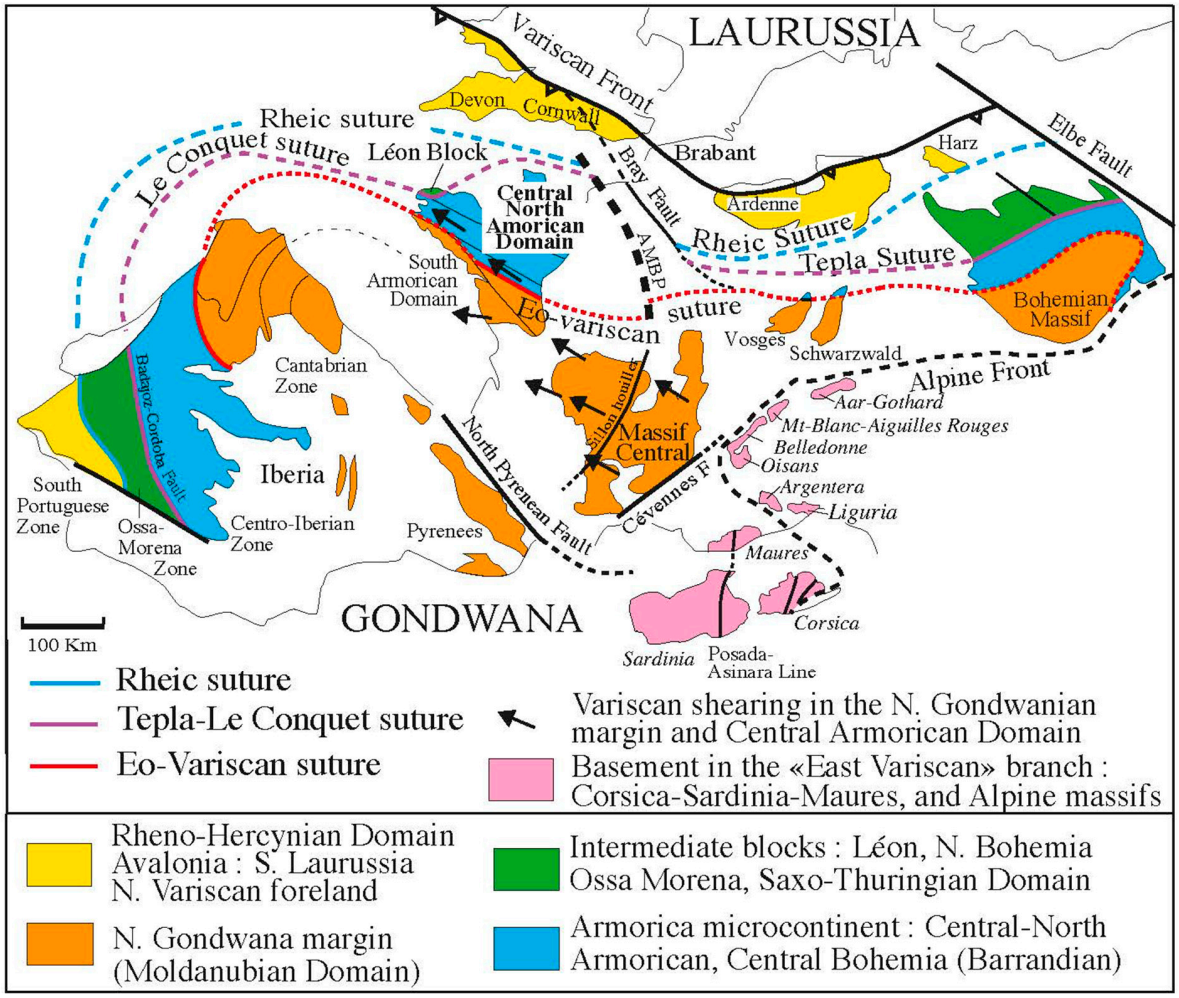

Figure 1. General tectonic framework of the European Variscan belt showing the ophiolitic sutures and microcontinents (from 17, and 27).

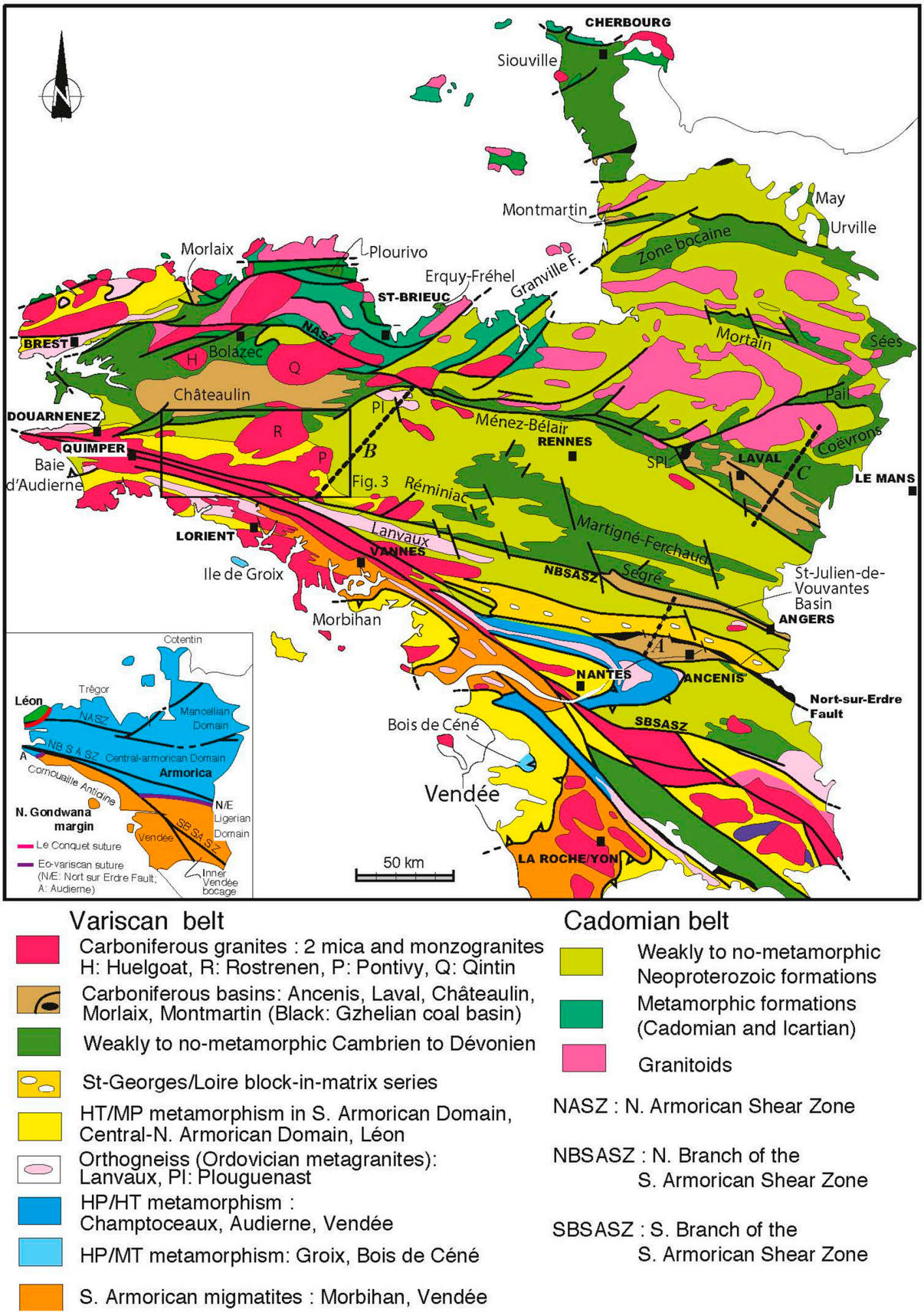

Figure 2. Structural map of the Armorican Massif with location of the study area (Figure 3) and trace of the three segments A, B, and C used to construct the synthetic general cross-section shown in Figure 13. Inset shows the subdivision of the Armorican Massif in three geodynamic domains, namely from north to south, the Léon, Armorica, and Northern Gondwana margin.

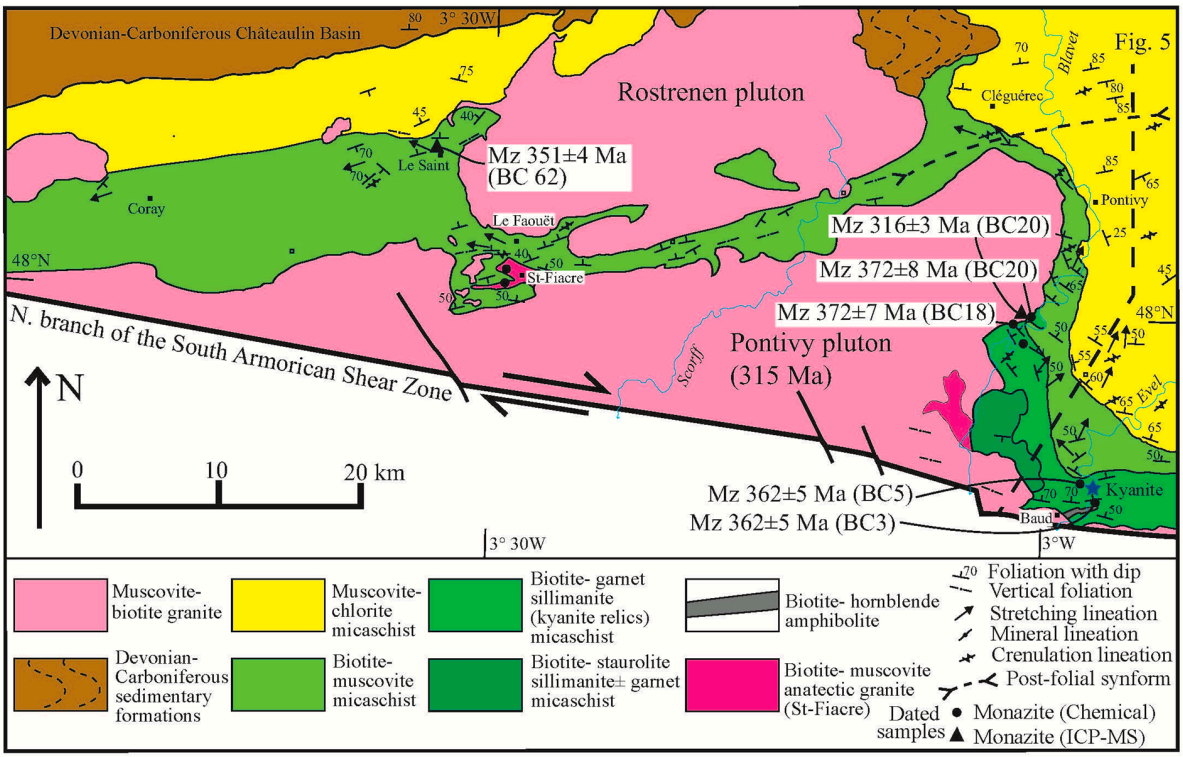

Figure 3. Geological map of the study area showing the metamorphic rocks in the southern part of the Central-North Armorican domain. The metamorphic zonation with decreasing conditions to the north or NE is well exposed to the SE of Pontivy. Monazite ages are also indicated.

Tectonically, in all the proposed models, Armorica was located in the upper plate, behaving as a rigid continental mass where the Variscan deformation and metamorphism are almost absent, except those related to strike-slip faults, and in the thermal aureoles of the post-collisional plutons that induce a thermal softening of the continental crust, e.g., [33–37]. In Central Brittany, the southern margin of Armorica exposes a medium pressure/medium temperature (MP/MT) barrowian-type metamorphism with biotite–garnet–staurolite ± kyanite assemblages recognized for a long time [38,39] but poorly considered in the tectonic models of the Variscan orogeny dealing with the French Armorican Massif. This feature does not comply with the view of a rigid Armorican microcontinent since the thermal conditions coeval with this metamorphic event will enhance a ductile behavior in the middle crust.

This paper aims to clarify the petrographic, structural, and geochronological constraints of the southern part of the Central Armorican domain. The geodynamic significance of these tectonic and metamorphic aspects will be discussed in the framework of the Variscan evolution of the Armorican massif. More generally, this study will also bring new general insights into the way the continental crust of the upper plate may behave in a collisional orogen.

2. Geological Setting

2.1. The Variscan Geodynamic Framework of the Armorican Massif

The structural pattern of the Armorican Massif is dominated by E-W to NW-SE striking dextral strike-slip faults of the North Armorican Shear Zone (NASZ) and South Armorican Shear Zone in the north and south of the massif, respectively (Figure 2). The latter split into a northern branch from Quimper to Angers and a southern one from Quimper to Nantes, itself subdivided in a horse-tail termination with several second-order faults. The SASZ is famous as the type-locality of S-C fabrics [40,41] but whatever the importance of the crustal-

scale strike-slip faults in the final architecture of the Armorican Massif, these structures do not bear a geodynamic significance for the Variscan evolution in terms of crustal thickening or microcontinent assemblage.

From a plate tectonics point of view, the Armorican massif must be separated into three domains, namely: (i) Léon, (ii) Central-North Armorica, and (iii) South Armorican domains (Figures 1 and 2). These three blocks are bounded by Le Conquet-Tepla and eo-Variscan ophiolitic sutures along which boudins of serpentinites, gabbro, amphibolites, mafic lavas, and siliceous metasediments interpreted as ophiolitic elements are sporadically exposed see for instance [17,18,42,43] for details. At the scale of the entire Variscan belt, the Léon, Central-North Armorican, and South Armorican domains are ascribed to the Saxo-Thuringian and Armorica microcontinents, and the northern margin of the Gondwana continent, respectively (Figures 1 and 2). The timing of the collision between Gondwana and Armorica, accommodated by a north-directed subduction and referred to as the eo-Variscan collision, is controversial. It might have occurred in the Late Devonian-Early Carboniferous [14,18] or in Early Devonian [17,44,45]. The boundary between Armorican and Saxo-Thuringian (or Léon domain) microcontinents is represented by the Le Conquet-Tepla ophiolitic suture (Figure 1). The collision between the two blocks was accommodated by a south-directed subduction, though its age is poorly constrained, an Early Carboniferous age is generally accepted [18,43].

2.2. The Armorica Microcontinent

The Central-North Armorican Domain (CNAD) exposes fossiliferous Paleozoic formations, e.g., [18,37,46–50]. The Cambrian, Ordovician, and Silurian formations unconformably cover Late Neoproterozoic (mostly Ediacaran) rocks deformed and metamorphosed during the Cadomian orogeny, e.g., [37,51]. Devonian rocks crop out mostly in the western part of the domain, near Brest, and in limited areas in the Châteaulin, Ménéz-Belair, Laval, Morlaix, and Ancenis basins [47,49]. Early–Middle Carboniferous (Tournaisian–Visean) formations are exposed close to the NASZ, from West to East, in the Châteaulin, Menez-Belair, and Laval basins [48,52,53].

In the Central-North Armorica domain, the most obvious Variscan deformation is characterized by upright folds, with or without an axial planar cleavage, and decollement layers coeval with folds and thrusts developed in the Paleozoic series overlying the Neoproterozoic Cadomian basement, and an important component of strike-slip shearing, e.g., [33–35,42,54–57].

Granitoids are widespread in the Central-North Armorican Domain [36,37,57–61]. Early Ordovician granites, now changed to orthogneiss, are exposed in Lanvaux, Plouguenast, Douarnenez, and Brest (Figure 2). These plutons are interpreted as emplaced during the Late Ordovician rifting that led to the separation of Armorica from Gondwana [17,44]. Late Carboniferous two-mica granites and granodiorites crop out as the Pontivy, Rostrenen, Huelgoat, and Quintin, to mention only the largest ones. Their location close to the NASZ and the SASZ suggests that they were emplaced during the dextral shearing, e.g., [36,37,41,61,62].

Due to the Late Carboniferous dextral shearing along the S. Armorican Shear Zone, the presently exposed southern boundary of Armorica does not correspond to its primary one. In the eastern part of the CNAD, the triangular area located between the Nort-sur-Erdre fault and the north branch of the S. Armorican Shear Zone is formed from South to North by the St-Georges-sur-Loire Unit and the Lanvaux unit, respectively, Figure 2; see [17,37,44] for details. More to the west, north of the North Branch of the South Armorican Shear Zone, MP/MT metamorphic rocks develop from the east of Pontivy to Douanenez to the west.

3. Petro-Structural Analyzes of the Metamorphic Series in the Pontivy–Coray Area

3.1. Bulk Architecture

North of the N. Branch of the SASZ, micaschists with subordinate amounts of amphibolite and quartzite are exposed in the Pontivy–Coray area, particularly along rivers such as the Blavet or Evel (Figure 3). As documented for a long time [35,38,39,63,64], the micaschists exhibit a progressive evolution in metamorphic mineral assemblages from the south to the north with (i) biotite–staurolite–sillimanite ± garnet to the NW of Baud, (ii) biotite–garnet–sillimanite, (iii) biotite–muscovite, (iv) muscovite–chlorite. At about 25 km northward, the chlorite–muscovite schists are replaced by Ordovician to Devonian black mudstone and sandstone. The protoliths of the metapelites are ascribed to the Ediacaran (formerly Brioverian). NW of Baud and near S^t-Fiacre, biotite–muscovite anatectic granitoids crop out, furthermore, between S^t-Fiacre and Le Faouet, muscovite–K-feldspath–sillimanite micaschists form the country rocks of the S^t-Fiacre massif (Figure 4D). This mineral assemblage supports a high-temperature event, but migmatites have not been observed. Boudinaged veins of two-mica granite develop within the foliation (Figure 4B). From Baud to the north, the foliation consistently dips to the NE with a dip angle progressively steepening from 50° to 85°. A similar pattern can be observed in the western part of the study area between S^t-Fiacre and Le Saint (Figure 3). In the narrow corridor between the Pontivy and Rostrenen plutons, the foliation keeps the same NE-SW strike but with a steeper attitude, sometimes subvertical. North of Cléguérec, the changing dip in the muscovite–chlorite micaschist suggests that this area corresponds to a km scale post-folial synform, several second-order synforms and antiforms are likely. Therefore, the bulk geometry of the metamorphic foliation observed in the Pontivy area depicts the structure of an N-dipping, E-W trending half-dome structure. The southern part of this dome is abruptly cut by the N. branch of the SASZ (Figure 5). The Pontivy biotite–muscovite leucogranite that yields a zircon U/Pb age at ca.315 Ma intrudes the metamorphic series at a high angle with respect to the foliation and isograds [60,63]; Figure 3.

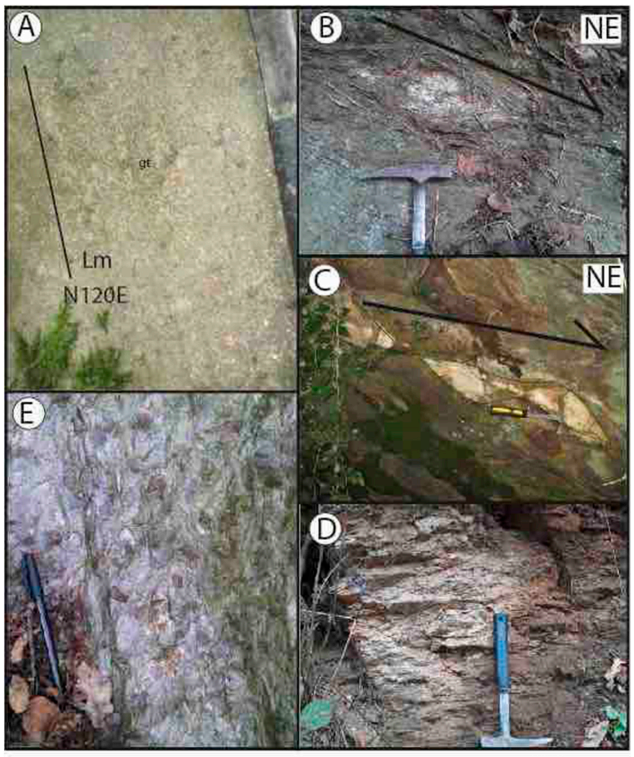

Figure 4. Field pictures. (**A**): Biotite–muscovite–garnet(gt)–quartz micaschits; quartz pressure shadows around garnet define a NW-SE striking mineral and stretching lineation (Evel valley, N47°53′19″,

W2°58′20″); (**B**): Top-to-the-NE leucogranite boudin (Evel valley, N47°53′18.5″, W2°58′20″); (**C**): Top-to-the NE sigmoidal quartz vein (Evel valley, N47°53′193″, W2°58′19″); (**D**): Biotite–muscovite–sillimanite micaschist (SE of Le Faouet, N47°53′19″, W2°58′19″); (**E**): cm sized staurolite porphyroblast cutting the regional foliation (Blavet valley, N. of St-Nicolas-des-Eaux, N47°56′20″; W3°1′22″).

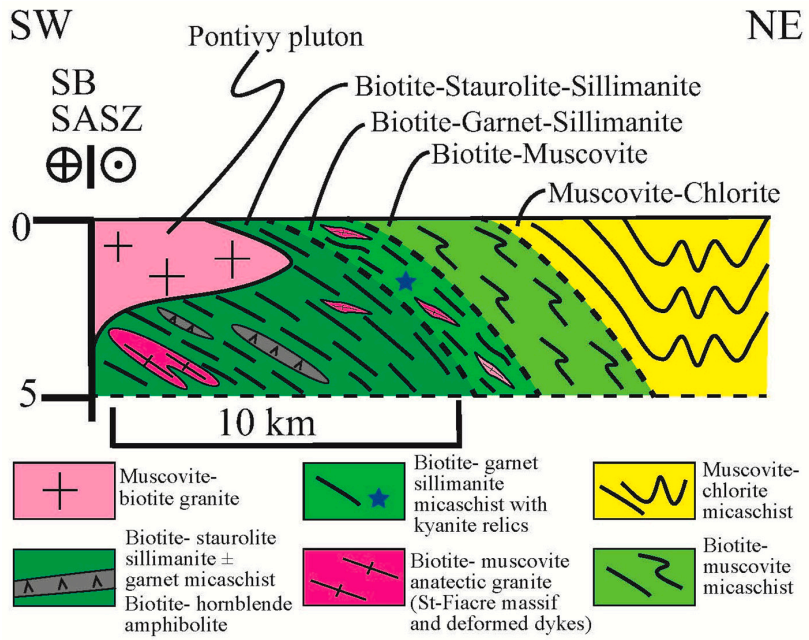

Figure 5. Cross-section of the study area (see location in Figure 3). The geometry of the foliation defines a domal structure, the core of which is occupied by anatectic granites but cross-cut by the Pontivy two mica pluton.

3.2. Microstructural Observations

The regional foliation, S1, is defined by the preferred orientation of quartz, biotite, and muscovite in the micaschists. North of Pontivy, the foliation develops within low-grade (chlorite–muscovite) micaschists. In some places, sedimentary structures (e.g., laminae, irregular silty layers) corresponding to the initial bedding are still preserved. Thus, this surface can be referred to as S0-S1. S0-S1 is microfolded by NE-SW striking (in average N40E) upright folds. At the regional scale, a crenulation lineation is coeval with a km scale NE-SW striking synform that probably extends in the biotite–muscovite micaschist corridor developed between the Pontivy and Rostrenen plutons. A similar crenulation lineation is recognized in the Evel and Blavet valleys between Pontivy and Baud.

Both S1 and S0-S1 surfaces contain two linear microstructures: firstly, a mineral and stretching lineation (L1) represented by quartz pressure shadows along garnet (Figure 4A) and elongated biotite or muscovite; secondly, the S1 foliation is cut by shear bands with discrete slickenlines (L2) marked by N-S to NNE-SSW striking white mica and sigmoidal quartz-FK porphyroblasts (Figure 4C). Although the direct microstructural superimposition evidence is lacking, the discrete non-penetrative character of the slickenlines suggests that this microstructure developed after the formation of the penetrative NW-SE (N120E) striking mineral and stretching (L1) lineation. The formation of the NW-SE stretching lineation was likely coeval with the S1 foliation during a single tectono-metamorphic event. Moreover, south of Cléguérec (Figure 3), the S0-S1 surface, deformed by upright crenulation folds, contains opaque minerals with quartz pressure shadows, the asymmetry of which indicates a top-to-the-NW sense of shear (Figures 6 and 7J).

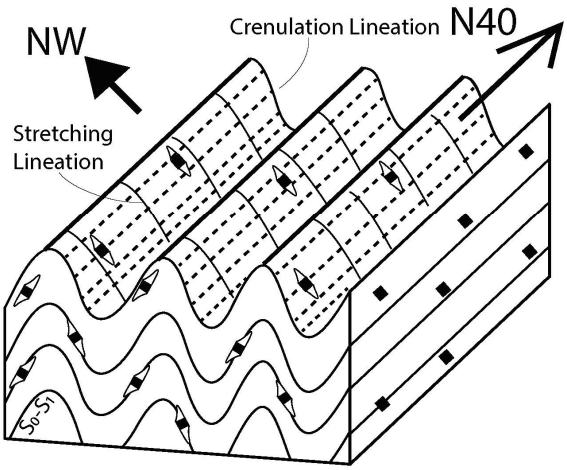

Figure 6. Three-dimensional diagram showing the regional foliation folded by N40E striking microfolds with axes parallel to a crenulation lineation. The foliation also shows a folded NW-SE striking mineral lineation with pressure shadows along opaque grains. Before microfolding, the pressure shadow asymmetry indicates a top-to-the-NW sense of shear. The section perpendicular to the microfolds corresponds to Figure 7J.

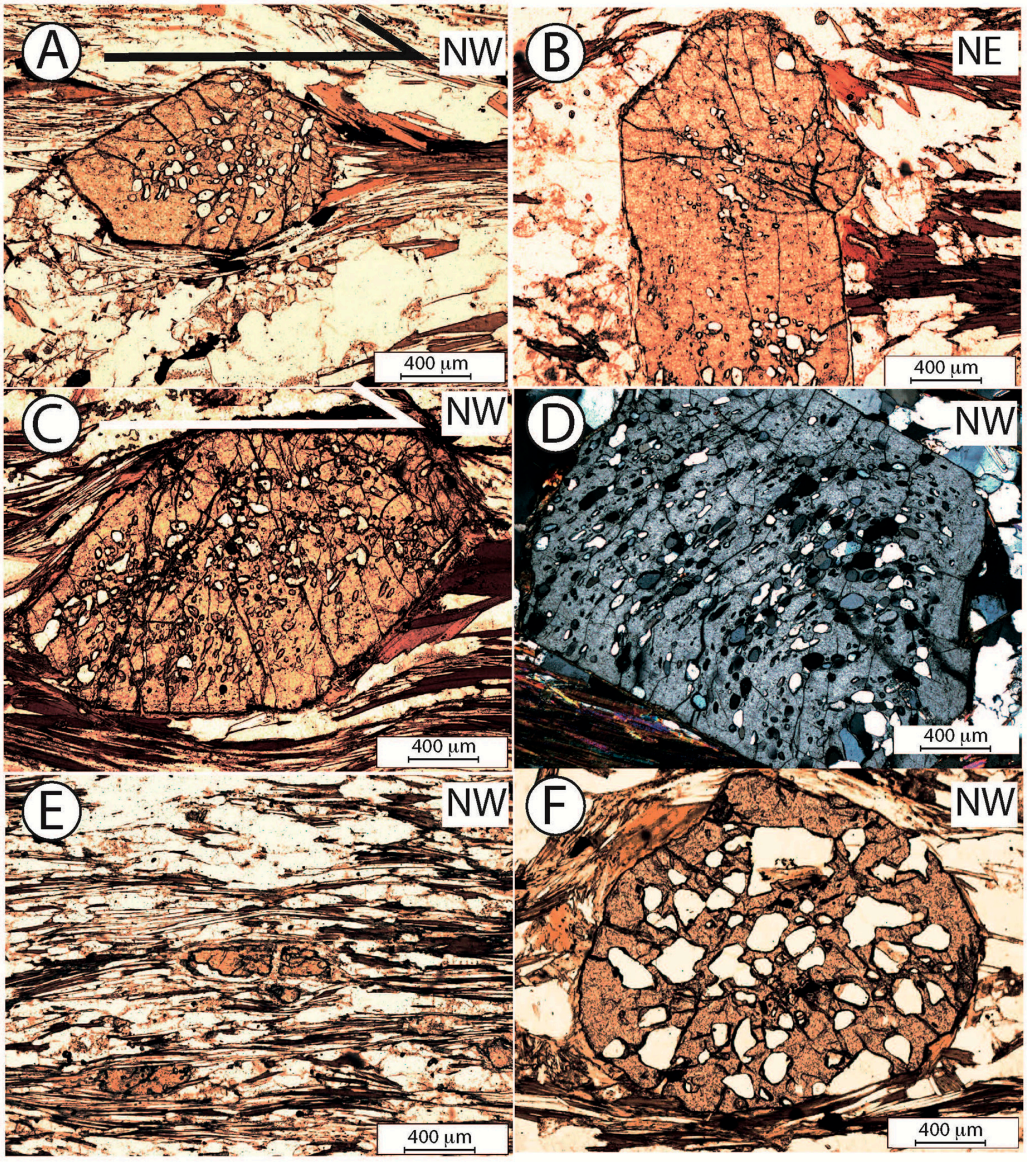

Figure 7. *Cont.*

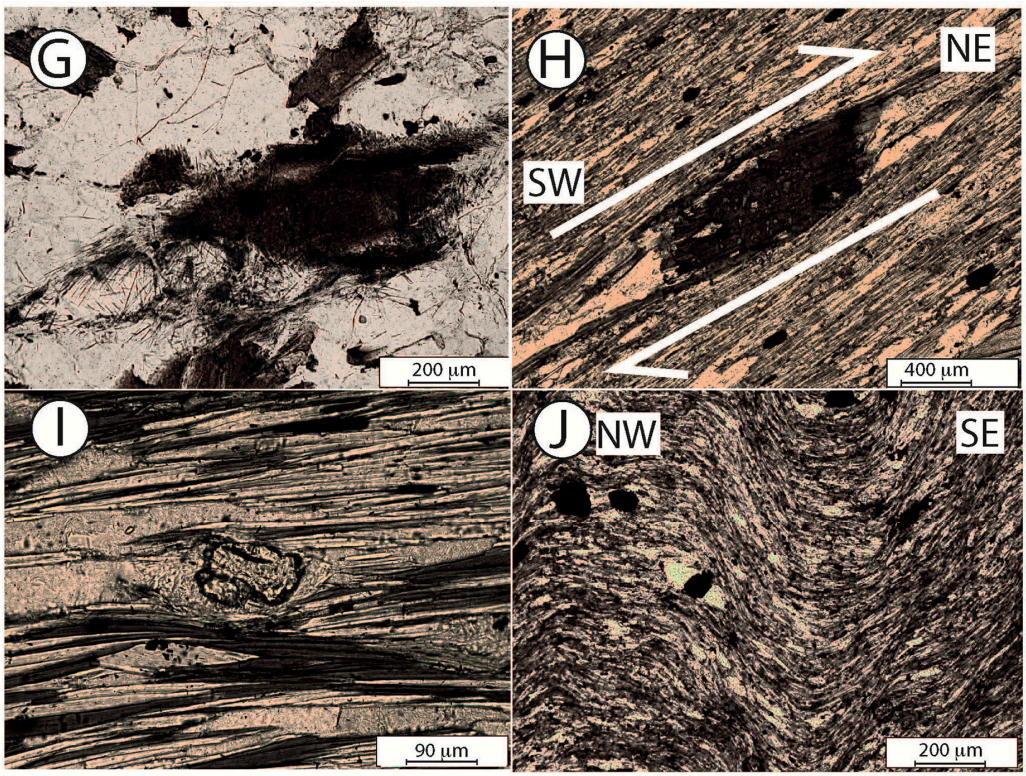

Figure 7. Thin section pictures. (**A**–**F**) images come from biotite–staurolite ±garnet micaschists sampled within a few tenths of meters in the Evel valley (N47°53′16″, W2°58′15.7″). (**A**): Staurolite with random quartz inclusions and asymmetric biotite pressure shadows indication a top-to-the-NW shearing; (**B**): Same sample as A but cut perpendicular to the lineation showing a staurolite porphyroblast at high angle to the regional foliation; (**C**): Staurolite with quartz inclusion and biotite pressure shadows indicating a top-to-the NW sense of shear; (**D**): Staurolite with quartz inclusion defining a folded internal foliation unrelated with the regional one, suggesting the existence of an earlier foliation. Note the sharp boundary in the bottom of the staurolite grain; (**E**): Small-sized staurolite grain parallel to the regional foliation; (**F**): Garnet porphyroblast with randomly arranged quartz inclusion without internal foliation. (**G**): Biotite–muscovite–fibrolitic sillimanite micaschist (S. of St-Caradec, N48°1′35″, W3°20′48″); (**H**): Sigmoidal biotite showing a dextral sense of shear consistent with the Armorican shear zone (N48°51′35″, W3°38′21″); (**I**): Kyanite relict indicative of an earlier metamorphic event of higher pressure conditions than the main barrowian one. The grain is surrounded by a sericite halo elongated in the NS-SW direction (N47°53′16.5″, W2°58′16″); (**J**): Crenulated biotite–chlorite micaschist, observed in XZ section. The folded foliation contains opaque minerals fringed by quartz pressure shadows (Cléguerec, N48°7′6″, W3°5′13″; see also Figure 7).

3.3. The Place of the Staurolite and Garnet Porphyroblasts Crystallization in the Deformation Succession

Garnet and staurolite are the most spectacular metamorphic porphyroblasts crystallized in the Pontivy–Coray area. The relationships between the deformation and crystallization allow us to recognize several episodes of porphyroblast crystallization with respect to foliation development. The largest staurolite porphyroblasts, up to 2 or 3 cm long, are superimposed, often obliquely, to the foliation (Figure 4E). In the thin section, these porphyroblasts that contain a few quartz inclusions have a sub-idiomorphic habitus (Figure 7B). They are considered crystallized after the main regional deformation event or in its latest increments. Other mm sized staurolite grains are arranged within the regional foliation, and biotite pressure shadows develop along the stretching lineation (Figure 7A,C). Most of the quartz inclusions in these porphyroblasts do not show any preferred orientation. A similar observation can be made for garnet porphyroblasts. Thus, this generation of

staurolite and garnet can be considered as crystallized during the main stage, or increment, of the formation of the S1 foliation. The asymmetric pressure shadows indicate a top-to-the-northwest shearing. Lastly, some small-sized staurolite porphyroblasts (around 0.5–0.2 mm), also parallel with the S1 micas, are boudinaged along the NW-SE lineation. These grains can probably be considered as formed during the S1 foliation development.

Kyanite is also recognized in the Pontivy-Corray area. In agreement with previous authors [38,39,65], two types of habitus are recognized for kyanite. The most spectacular one consists of pluricentimeter-size fibrous bluish crystals related to fluid circulations, possibly developed in the late stages of two-mica granite emplacement. Moreover, the second type, represented by ca 50 to 70 µm size synfolial grains surrounded by a white mica (possibly sericite?) halo included in the regional foliation (Figure 7I), argues for an earlier middle- to high-pressure event that preceded the main MP/MT event. It is also worth noting that, in a few staurolite grains along the Evel valley, the porphyroblasts exhibit curved quartz inclusions that suggest the existence of an earlier folded foliation. Moreover, S. of Coray, the cm size post-folial staurolite porphyroblasts contain ilmenite inclusions with quartz trails oriented at a high angle from the quartz inclusions in staurolite (Figure 8). Furthermore, south and east of Le Faouet, muscovite–K-feldspath–sillimanite micaschists that form the country rocks of the S^t-Fiacre anatectic granitic massif indicate that this area experienced an HT event (Figure 7G).

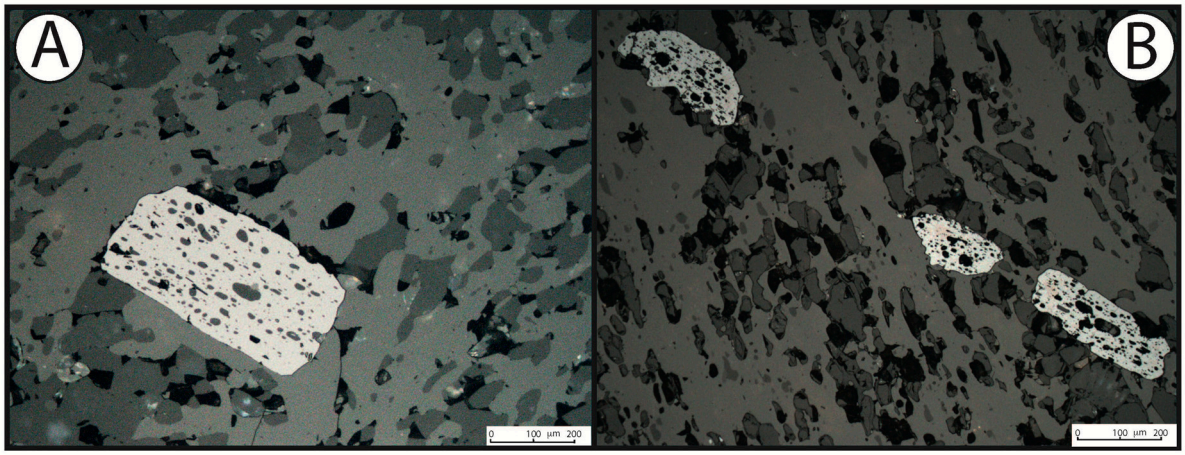

Figure 8. BSE images of ilmenite included in post-folial staurolite porphyroblast near Coray (N 40°2′33″, W 3°50′44″). (**A**): The ilmenite grain shows quartz inclusions oriented at a high angle from the quartz inclusions in staurolite; (**B**): aligned ilmenite grains with quartz inclusions oriented at a high angle from the quartz inclusions in staurolite.

In summary, the microscopic observation of staurolite and garnet porphyroblasts document the fact that these porphyroblasts are syn- to post-folial grains that crystallized all along the deformation history during the main MT/MP metamorphic event. In addition, the presence of relict kyanite and older foliations preserved as inherited inclusion trails suggest that the metamorphic series of the Pontivy–Coray area experienced higher pressure conditions than those indicated by the muscovite–K-feldspar–sillimanite assemblage. In the following, the main MT/MP metamorphism will be referred to as the M1 event; however, the kyanite relicts will be called M0, although they are probably an earlier increment of the same M1 event.

3.4. Thermo-Barometric Evolution

Thermo-barometric estimates of the conditions experienced by the metamorphic rocks of the Pontivy–Coray area have been carried out [63]. According to these authors, a first assemblage, coeval with the regional foliation, developed under MT/MP conditions with

slightly changing P and T values depending on the sample location in the Evel or Blavet valleys (Figure 9). The same study documents a decompression heating evolution from 0.85 GPa-500 °C in the Blavet River to 0.6–0.5 GPa-700 °C near Le Faouet. This result complies with the presence of muscovite–sillimanite–K-feldspar micaschists that suggest incipient migmatization in this latter area but not in the former ones. At ca 700 °C, one may expect pervasive melting of the hydrated pelitic rocks that are not observed both in the field or in thin sections. Nevertheless, this P-T evolution is at variance with the LP/HT conditions (ca. 0.25–3 GPa, 500–700 °C) measured in the biotite–garnet–andalusite hornfelses. Schulz et al. [61] also interpreted the regional MP/MT metamorphic evolution as a consequence of crustal thickening. Indeed, the occurrence of kyanite relics, NE of Baud, supports the interpretation that the micaschists underwent high-pressure conditions at ca. 0.9–1 GPa, (400–500 °C) before the MP/MT (M1) event.

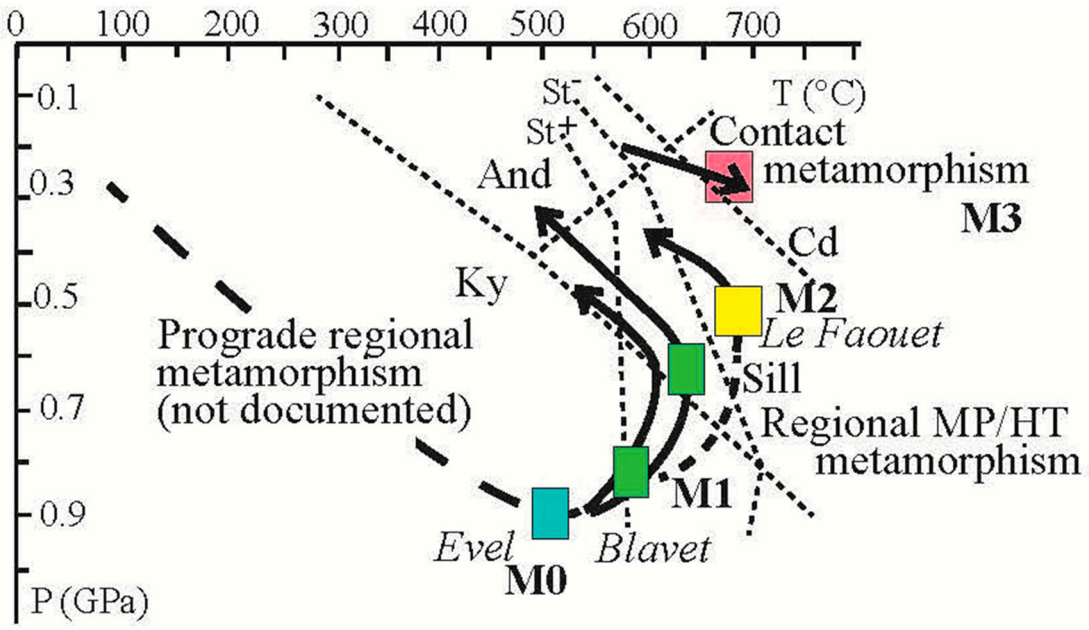

Figure 9. P-T path experienced by the metamorphic rocks of the Pontivy area (modified from 63). The P-T paths document an early metamorphic event (M0), presently preserved as kyanite relics, followed by a regional MP/MT event (M1) with biotite–garnet–staurolite, then a metamorphic decompression heating, up to a muscovite–sillimanite–K-feldspar stage (M2). This evolution is independent of the HT/LP contact metamorphism event (M3) developed during the pluton intrusions.

As already well documented [63], the andalusite–garnet assemblage developed in the contact metamorphism aureole around the Pontivy and Rostrenen plutons yields pressure and temperature conditions of 0.25–0.3 Gpa and 500–700 °C, respectively. These values are distinctly different from those established for the regional metamorphism (Figure 9). In conclusion, the thermo-barometric estimates document an early metamorphic event (M0), presently only preserved as kyanite relics, and possible inclusion trails in some staurolite porphyroblasts. M0 was followed by a regional MP/MT event, characterized by a biotite–garnet–staurolite assemblage (M1), then by a metamorphic decompression heating with a muscovite–sillimanite–K-feldspar assemblage (M2). This evolution is independent of the HT/LP contact metamorphism event (M3) developed during the granitic intrusions.

4. Geochronological Constraints

In order to place time constraints on the metamorphic and structural evolution of the Pontivy–Coray area depicted in the previous sections, monazite dating has been carried out. This mineral is conspicuously observed in metapelites that underwent MP/MT

metamorphic conditions. It thus provides access to the age of metamorphism experienced by metapelites, whereas low-temperature dating, such as the mica $^{40}Ar/^{39}Ar$ method, is sensitive to thermal resetting induced by nearby plutons. In the study area, monazite occurs either as single gains isolated in the micaschist foliation or as inclusions in biotite and muscovite. The size of the analyzed grains ranges from 50 to 150 µm with sub-euhedral or anhedral habitus (Figure 10). Since some grains are fringed by pressure shadows, they experienced the ductile deformation coeval with the MP/MT event; thus, it is reasonable to consider that they crystallized or re-crystallized during the M1 metamorphism coeval with the regional deformation, even if some monazite grains might be inherited from the Neoproterozoic protolith.

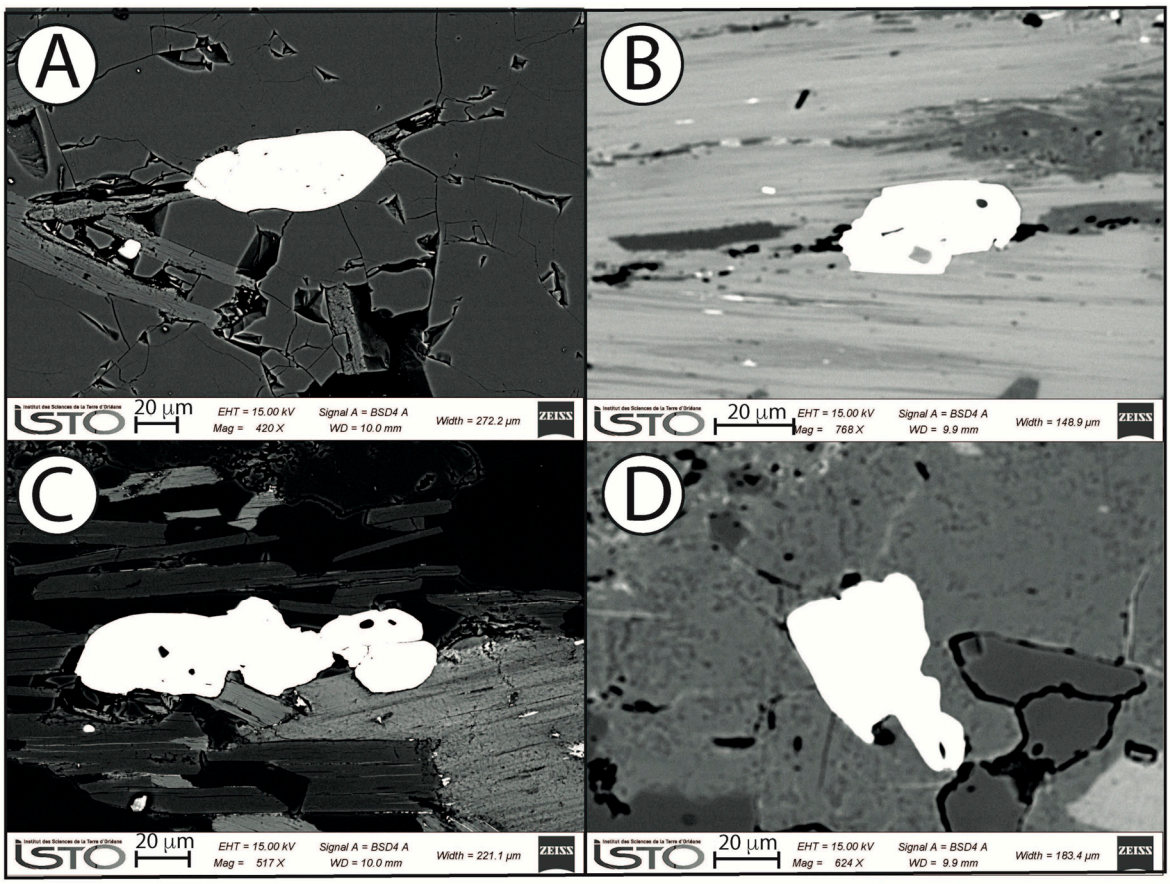

Figure 10. Monazite BSE images of representative grains dated by U/Th/Pb method. (**A**): BC3; (**B**): BC5; (**C**): BC 18; (**D**): BC19 (location in Figure 3).

4.1. U-Th-Pb Chemical Dating

Owing to its high U and Th contents and often negligible common lead, monazite chemical dating is a fast and cheap method to investigate metapelites metamorphosed in MP/MT conditions, e.g., [66–69]. In situ measurements in thin sections have been realized following the method developed by Suzuki and Adachi [66] and Cocherie et al. [68]. It has been extensively used in metapelites, migmatites, and granites in the Variscan French Massif Central. The analysis of monazite grains directly from polished thin sections was performed by a Cameca SX 50 EPMA co-operated by BRGM-CNRS-Orléans University. An accelerating voltage of 20 kV and a beam current of 100 nA were chosen as operating conditions. Synthetic phosphates, glasses, and natural minerals were used as standards. The counting times (2/3 on peak and 1/3 on background) vary from 20 s for Si, P, Ca, Nd, Gd, Y, Th, Ce, and La to 100 s for U and 120 s for Pb. Considering such parameters, the detection limit for Th, U, and Pb is 150 ppm; for detailed information on analytical

conditions, standards, and data processing, see [70–74]. The chemical dating is presented as average, following Suzuki and Adachi [66] (Figure 11). The sampling sites of the analyzed micaschists are located in Figure 3.

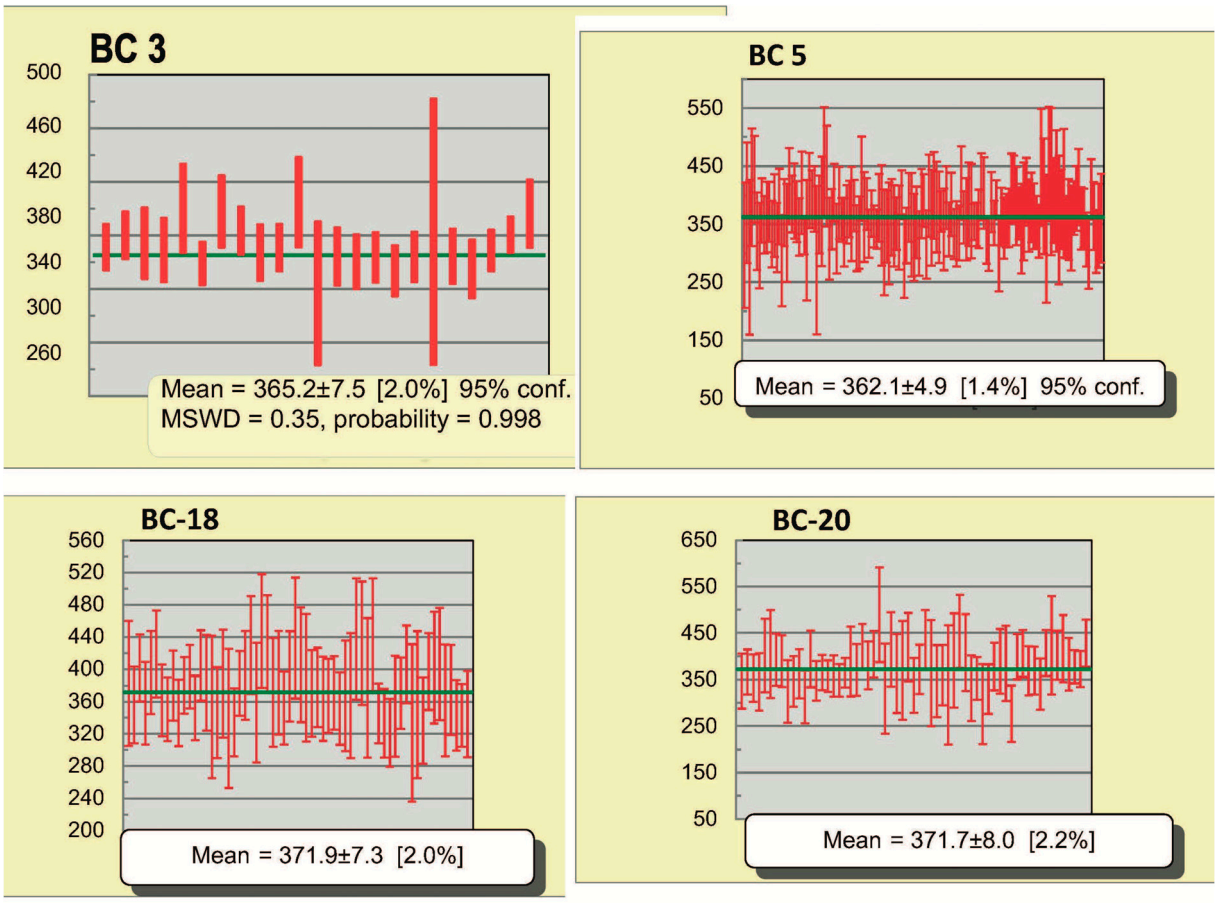

Figure 11. Monazite U-Th-Pb chemical ages of micaschists samples along the Evel valley BC 3 (N47°53′16″, W2°58′15.7″), BC 5 (N47°53′25″, W2°58′29″), BC 18 (N47°59′13.6″, W3°2′14.7″), and along the Blavet valley BC 20 (N47°55′19″, W3°1′14″).

Samples BC 3 and BC 5 are biotite–staurolite micaschists from the Evel Valley. The analyzed monazites yield the same U-Th-Pb chemical dates of 362 ± 5 Ma. Samples BC 18 and BC 20 from the Blavet Valley are biotite–garnet and biotite–garnet–staurotide micaschist, respectively. Both rocks yield the same date of 372 ± 7 Ma and 372 ± 8 Ma. The geological significance of these results will be discussed in Section 5.

4.2. LA-ICP-MS Dating

In situ dating of monazite in biotite–sillimanite–K-feldspar–muscovite micaschist (BC 62), sampled north of Le Saint (Figure 3), was carried out on polished thin sections. Ablation was performed directly in thin sections at the GeOHeLiS analytical platform (University of Rennes) using an Excimer Laser System powered by an ultra-short pulse Coherent ExciStar XS (ESI NWR193UC) operating at a wavelength of 193 nm and consisted of 8 µm spot diameters produced with a repetition rate of 2 Hz. Ablated material was carried to the mass spectrometer in He (0.76 L/min) and then mixed with N (0.03 L/min) and Ar (0.67 L/min) before being introduced to the ICP source of an Agilent 7700x quadrupole ICP-MS equipped with a dual pumping system to enhance sensitivity. Tuning of the instrument and mass calibration were performed before the analytical session using the NIST SRM 612 reference glass, by monitoring the ^{238}U signal and minimizing the ThO+/Th+ ratio

(<0.5%). Analyses consisted of the acquisition of the ^{204}(Pb + Hg), ^{206}Pb, ^{207}Pb, ^{208}Pb, ^{232}Th and ^{238}U signals. The ^{235}U abundance was calculated from the measured ^{238}U on the basis of a ^{238}U/^{235}U ratio of 137.818. Single analyses consisted of ~20 s of background integration with the laser off, followed by ~60 s integration with the laser firing and then a ~ 10 s delay for wash out. Raw data were corrected for Pb/U and Pb/Th laser-induced elemental fractionation and for instrumental mass discrimination by standard bracketing with repeated measurements of the monazite reference material Moacyr [75]. Along with the unknowns, the monazite Manangoutry [76] was measured to monitor the precision and accuracy of the analyses and produced a Concordia age of 544 ± 10 Ma (N = 5; MSWD = 0.6) during the course of the analyses. Data reduction was carried out with the Iolite software package [77]. The analyses were performed in time-resolved mode. More information about the analytical procedure can be found in Table 1, "Operating conditions for the LA-ICP-MA equipment" and in [78].

Table 1. Operating conditions for the La-ICP-Ms equipment.

Laboratory and Sample Preparation	
Laboratory name	GeOHeLiS Analytical Platform, OSUR, Univ of Rennes, France
Sample type/mineral	Monazite
Sample preparation	In thin-section
Laser ablation system	
Make, model and type	ESI NWR193UC, Excimer
Ablation cell	ESI NWR TwoVol2
Laser wavelength	193 nm
Pulse width	<5 ns
Fluence	3 J/cm^2
Repetition rate	2 Hz
Spot size	8 µm
Sampling mode/pattern	Single spot
Carrier gas	100% He, Ar make-up gas and N2 (3 mL/mn) combined using in-house smoothing device
Background collection	20 s
Ablation duration	45 s
Wash-out delay	15 s
Cell carrier gas flow (He)	0.76 L/min
ICP-MS Instrument	
Make, model and type	Agilent 7700x, Q-ICP-MS
Sample introduction	Via conventional tubing
RF power	1350 W
Sampler, skimmer cones	Ni
Extraction lenses	X type
Make-up gas flow (Ar)	0.67 L/min
Detection system	Single collector secondary electron multiplier
Data acquisition protocol	Time-resolved analysis

Table 1. *Cont.*

Laboratory and Sample Preparation	
Scanning mode	Peak hopping, one point per peak
Detector mode	Pulse counting, dead time correction applied, and analog mode when signal intensity >~10^6 cps
Masses measured	^{204}(Hg + Pb), ^{206}Pb, ^{207}Pb, ^{208}Pb, ^{232}Th, ^{238}U
Integration time per peak	10–30 ms
Sensitivity/efficiency	20,000 cps/ppm Pb (50 µm, 10 Hz)
Data Processing	
Gas blank	20 s on-peak
Calibration strategy	Moacyr monazite used as primary reference material, Manangoutry monazite used as secondary reference material (quality control)
Reference material info	Moacyr [75] Manangoutry [76]
Data processing package used	Iolite 4 [77]
Mass discrimination	Standard sample bracketing with ^{207}Pb/^{206}Pb, ^{206}/^{238}U, ^{208}Pb/^{232}Th normalized to reference material Trebilcock
Common Pb correction	No common Pb correction
Uncertainty level and propagation	Ages are quoted at 2 sigma absolute, propagation is by quadratic addition. Reproducibility and age uncertainty of reference material are propagated.
Quality control/validation	Manangoutry: 544 ± 10 Ma (MSWD = 0.6; n = 5)

The first sample (BC62), collected north of Le Saint (Figure 3), corresponds to biotite–muscovite–sillimanite–garnet micaschist. Eighteen monazite grains of several 100 µm size have been analyzed (Table 2). They yield high thorium (average 32,000 ppm) and uranium (average 2300 ppm) contents. Plotted in a Tera–Wasserburg concordia diagram (Figure 12), they plot in a concordant to discordant position due to the presence of a slight amount of common Pb. They define a lower intercept date of 352 ± 12 Ma (MSWD = 0.36) with a (^{207}Pb/^{206}Pb)0 = 0.85 compatible with the Pb evolution model of Stacey and Kramer [79].

Table 2. Analytical data of the ICP-MS analysis.

GeOHeLiS Platform, Université de Rennes				Data for Tera-Wasserburg Plot					Data for Wetherill Plot					Dates					
Identifier	**U ppm**	**Th ppm**	**Pb ppm**	**$^{238}U/^{206}Pb$**	**2se%**	**$^{207}Pb/^{206}Pb$**	**2se%**	**rho**	**$^{207}Pb/^{235}U$**	**2se%**	**$^{206}Pb/^{238}U$**	**2se%**	**Rho**	**$^{207}Pb/^{206}Pb$**	**2se (abs)**	**$^{206}Pb/^{238}U$**	**2se (abs)**	**$^{207}Pb/^{235}U$**	**2se (abs)**	**% conc**
BC20																				
S220519a-02.d	8266	32,327	528	20.06	7.5	0.05342	2.6	0.26	0.3597	5.4	0.04984	7.5	0.50	346	59	314	23	312	14	100.5
S220519a-03.d	3864	17,632	324	19.46	7.4	0.05073	2.7	0.41	0.3584	5.1	0.05139	7.4	0.34	227	63	323	23	311	14	103.9
S220519a-04.d	3110	19,071	349	20.34	7.5	0.05487	3.4	0.32	0.3749	5.4	0.04915	7.5	0.43	406	76	309	23	323	15	95.7
S220519a-05.d	5532	27,567	430	19.56	7.8	0.05267	3.8	0.49	0.3701	5.8	0.05114	7.8	0.43	314	87	322	25	320	16	100.5
S220519a-06.d	3889	18,530	313	19.83	7.4	0.05220	2.7	0.40	0.3694	5.1	0.05042	7.4	0.36	293	63	317	23	319	14	99.3
S220519a-07.d	6314	46,556	700	20.12	8.2	0.05260	3.6	0.40	0.3552	6.1	0.04969	8.2	0.50	311	82	313	25	309	16	101.3
S220519a-08.d	4014	19,572	320	19.32	8.9	0.05381	4.5	0.51	0.3697	6.7	0.05175	8.9	0.68	362	102	325	28	319	18	101.8
S220519a-09.d	4076	61,299	997	19.88	7.7	0.05517	3.6	0.98	0.3800	5.6	0.05029	7.7	0.39	418	80	316	24	327	16	96.7
S220519a-10.d	3158	33,397	552	21.15	7.6	0.05586	3.9	0.01	0.3689	5.7	0.04729	7.6	0.03	446	87	298	22	319	16	93.4
S220519a-11.d	4773	31,334	550	20.26	7.4	0.05449	2.7	0.33	0.3735	5.2	0.04937	7.4	0.47	390	60	311	22	322	14	96.4
S220519a-12.d	4148	29,278	463	20.22	7.4	0.05211	2.7	0.46	0.3573	5.1	0.04946	7.4	0.46	289	63	311	22	310	14	100.3
S220519a-13.d	2305	13,115	220	19.26	7.4	0.05497	3.5	0.02	0.3843	5.3	0.05192	7.4	0.00	410	77	326	24	330	15	98.8
S220519a-14.d	2752	15,439	259	18.95	7.6	0.05097	3.7	0.39	0.3636	5.6	0.05276	7.6	0.42	239	86	331	25	315	15	105.2
S220519a-15.d	3137	34,412	521	19.33	8.1	0.05484	4.7	0.44	0.3760	6.3	0.05172	8.1	0.43	405	105	325	26	324	17	100.3
S220519a-16.d	2663	31,728	513	18.71	7.9	0.05262	4.8	0.50	0.3815	6.1	0.05344	7.9	0.40	311	109	336	26	328	17	102.3
S220519a-17.d	4542	35,473	566	19.97	7.5	0.05142	2.7	0.46	0.3504	5.2	0.05007	7.5	0.53	259	62	315	23	305	14	103.3
S220519a-18.d	3661	54,693	877	19.80	7.4	0.05473	3.0	0.19	0.3760	5.3	0.05051	7.4	0.51	400	67	318	23	324	15	98.0
S220519a-19.d	3185	26,703	421	20.23	7.6	0.05142	4.2	0.42	0.3500	5.7	0.04943	7.6	0.29	259	96	311	23	305	15	102.1
S220519a-20.d	5665	14,883	253	19.94	7.4	0.05205	2.7	0.37	0.3592	5.2	0.05015	7.4	0.48	287	63	315	23	312	14	101.2
S220519a-21.d	4499	49,067	777	20.32	7.5	0.05158	3.1	0.39	0.3497	5.3	0.04922	7.5	0.39	266	72	310	23	304	14	101.7
BC62																				
S220519a-23.d	3564	39,093	686	18.12	7.6	0.06024	3.5	0.49	0.4486	5.4	0.05519	7.6	0.32	611	75	346	26	376	17	92.0
S220519a-24.d	3222	24,048	419	18.37	7.6	0.05718	3.8	0.48	0.4240	5.6	0.05444	7.6	0.26	498	83	342	25	359	17	95.2
S220519a-25.d	2223	39,703	776	17.82	7.5	0.05440	3.5	0.42	0.4267	5.3	0.05612	7.5	0.29	387	79	352	26	361	16	97.5
S220519a-26.d	2628	15,781	286	17.70	7.7	0.05568	3.7	0.23	0.4358	5.7	0.05651	7.7	0.18	439	83	354	26	367	18	96.5
S220519a-27.d	2450	45,502	798	17.56	7.7	0.05825	3.9	0.47	0.4661	5.8	0.05693	7.7	0.36	538	86	357	27	389	19	91.9
S220519a-28.d	2609	48,838	821	17.53	7.8	0.05857	4.4	0.40	0.4577	6.0	0.05703	7.8	0.33	550	96	358	27	383	19	93.4
S220519a-29.d	1646	20,034	395	17.44	7.7	0.05810	4.8	0.43	0.4551	6.0	0.05735	7.7	0.28	533	105	359	27	381	19	94.4
S220519a-30.d	2612	42,238	777	17.49	7.6	0.06510	4.9	0.03	0.4978	6.7	0.05718	7.6	0.48	777	103	358	27	410	23	87.4
S220519a-31.d	1628	30,068	540	17.72	7.9	0.06010	5.5	0.19	0.4603	6.9	0.05643	7.9	0.31	606	120	354	27	384	22	92.0
S220519a-32.d	2448	37,859	676	17.90	7.4	0.05942	3.3	0.11	0.4519	5.3	0.05585	7.4	0.40	582	71	350	25	379	17	92.5
S220519a-33.d	1085	16,395	372	17.59	7.5	0.05603	4.8	0.39	0.4296	5.7	0.05685	7.5	0.25	453	106	356	26	363	17	98.2
S220519a-34.d	2050	36,117	670	16.80	7.6	0.05656	5.1	0.05	0.4537	6.3	0.05953	7.6	0.04	473	113	373	28	380	20	98.1
S220519a-35.d	1117	20,576	480	17.25	7.5	0.05808	4.5	0.35	0.4556	5.6	0.05799	7.5	0.32	532	99	363	26	381	18	95.3
S220519a-36.d	1861	18,574	365	17.68	7.5	0.05660	4.0	0.43	0.4357	5.6	0.05655	7.5	0.27	475	89	355	26	367	17	96.6
S220519a-37.d	1919	47,271	810	18.29	7.4	0.05629	3.6	0.43	0.4268	5.3	0.05467	7.4	0.34	463	80	343	25	361	16	95.1
S220519a-38.d	2651	19,238	338	18.24	7.6	0.05926	5.9	0.07	0.4584	8.0	0.05482	7.6	0.32	576	128	344	25	383	26	89.8
S220519a-39.d	3283	54,645	982	17.23	9.8	0.06019	6.0	0.33	0.4839	8.4	0.05804	9.8	0.70	609	129	364	35	401	28	90.7
S220519a-40.d	2429	15,879	294	17.85	7.5	0.05178	3.6	0.38	0.4024	5.4	0.05602	7.5	0.35	274	83	351	26	343	16	102.3

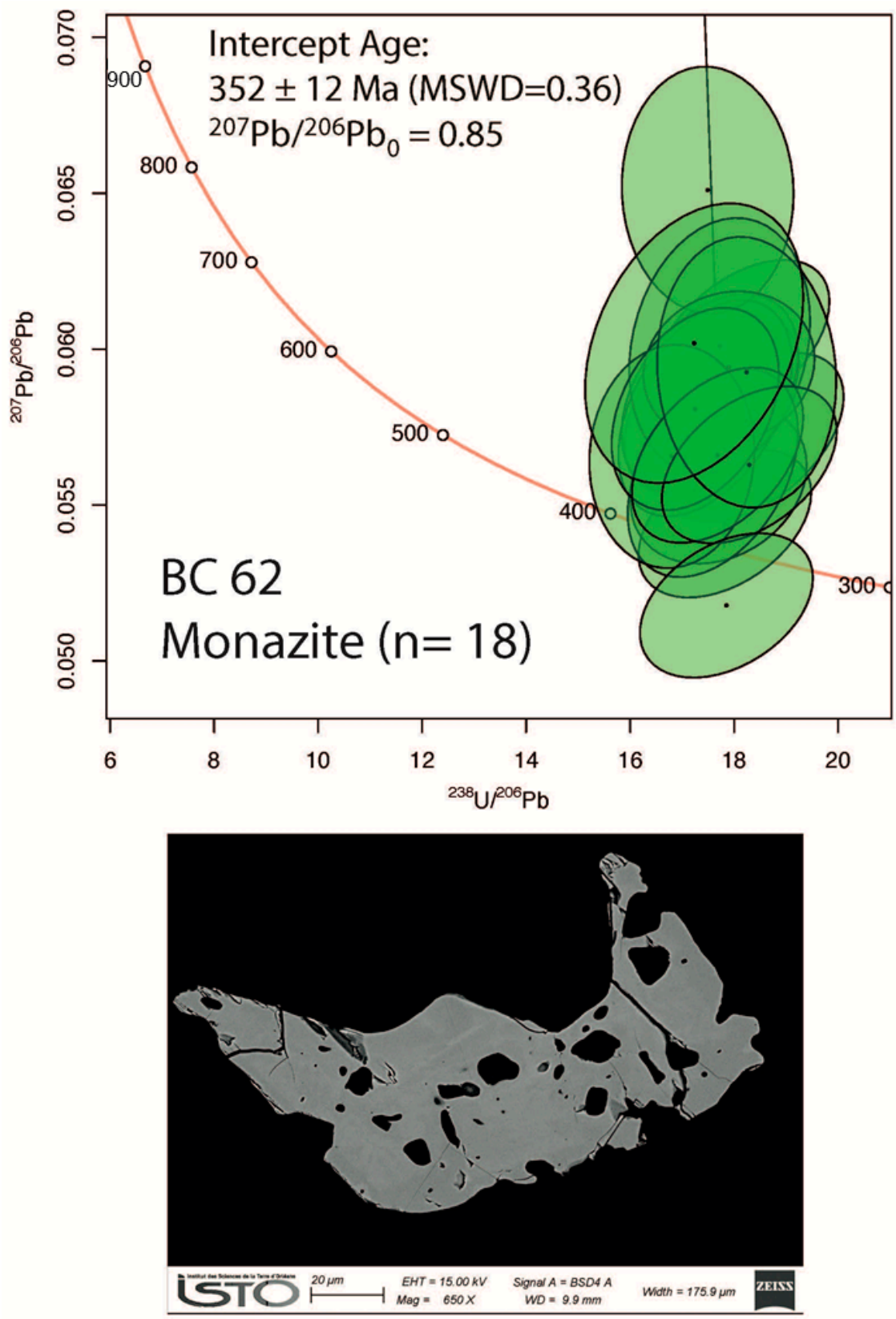

Figure 12. *Cont.*

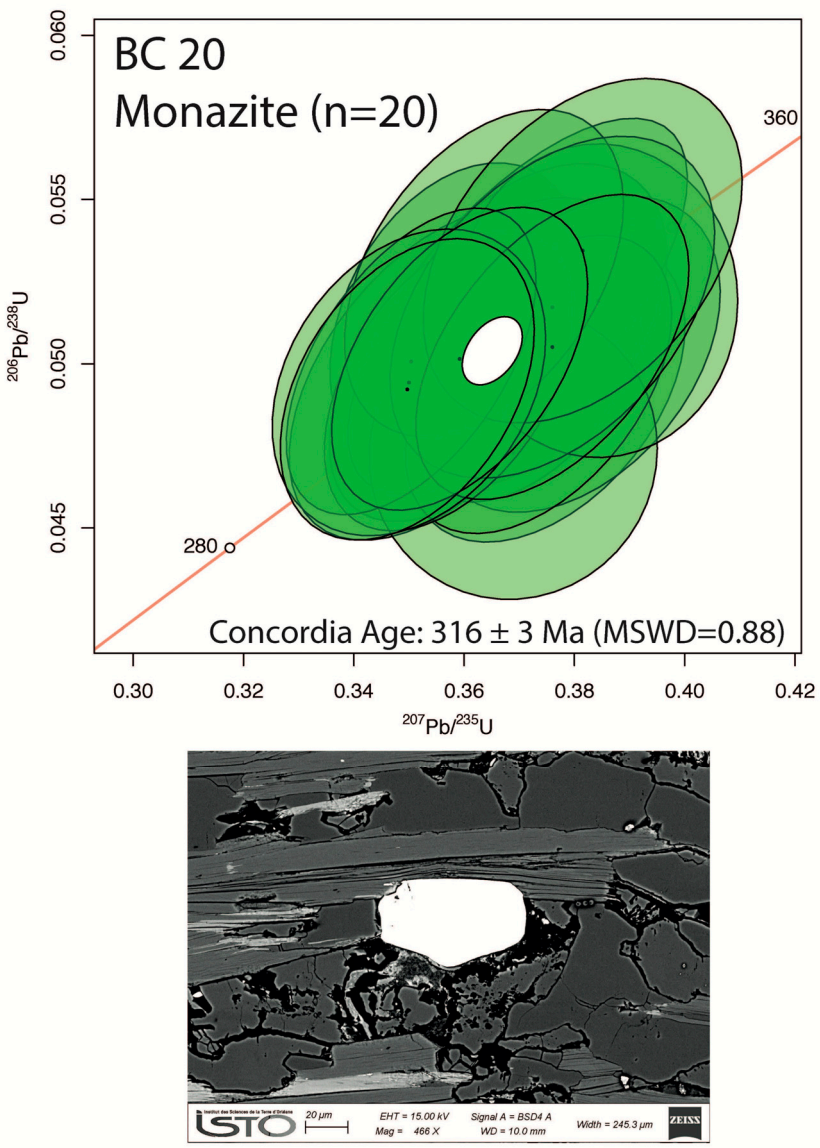

Figure 12. Tera–Wasserburg diagram of monazite analyzed by ICP-MS method in micaschist BC 62, north of Le Saint (located in Figure 3; N48°6′7″, W3°33′41″). BSE image of one analyzed grain. Concordia diagram of monazite analyzed by ICP-MS method in micaschist BC 20 in the Blavet Valley (located in Figure 3; N47°55′19″, W3°1′14″). BSE image of one analyzed grain.

The second sample, BC20, is biotite–garnet–staurolite micaschist, sampled in the Blavet Valley (Figure 3). Twenty monazite grains have been analyzed and present high thorium (average 30,600 ppm) and uranium (average 4200 ppm) contents. Plotted in a Wetherill Concordia diagram (Figure 12), they all plot in a concordant position and yield a concordant date of 316.2 ± 3.2 Ma (MSWD (Conc + Equiv) = 0.88). The interpretation of the monazite LA-ICP-MS dating results will be discussed in the next section.

5. Discussion

5.1. The Geological Significance of the Monazite U-Th-Pb Chemical and LA-ICP-MS Dates

Though the basis of the monazite chemical dating method is based on the postulate that common Pb is negligible, this assumption is not always fulfilled. The two micaschists (BC 18, BC 20) sampled along the Blavet Valley yield the same chemical date at ca. 372 Ma, this result appears quite old considering the geological record of the Armorican Massif, e.g., [18]. This old date might be due to important content in common lead. In the Evel

Valley, samples BC3 and BC5 yield comparable dates within uncertainty at ca. 362 Ma (Famennian) that might be considered for the age of the M1 metamorphic event, but a significant amount of common lead that would shift the dates toward older values cannot be discarded.

The presence of a non-negligeable amount of common Pb is confirmed by the ICP-MS analyses as one can notice in the monazite from sample BC62 (see earlier). Although it is possible to obtain a reliable age when conducting LA-ICP-MS analyses, even if the mineral does contain some common Pb (with the use of the Tera–Wasserburg diagram), it is not possible to do the same with chemical dating.

In this study, the ICP-MS monazite date of 352 ± 12 Ma from the biotite–sillimanite–K-feldspar–muscovite micaschist (BC 62) seems, therefore, more reliable, and this date is retained as geologically significant. The 316 ± 3 Ma age of sample BC20 is similar to the zircon LA-ICP-MS age of the Pontivy granite [60]. If this scenario is valid, the dates obtained by chemical dating should be discarded as they are not geologically significant.

5.2. The Pre-Late Carboniferous Structure of Armorica

In the Pontivy–Coray area, kyanite relics, formed during an MP/MT event (M0-M1), represent the earliest metamorphic event experienced by the Central-North Armorican Domain during the Variscan orogeny. The monazite age of 352 ± 12 Ma of the muscovite–sillimanite micaschists (BC 62) is in agreement with the thermal event (D2/M2) that was superimposed on the MP/MT one.

Metamorphic rocks are also recognized N. of Pontivy in the Plouguenast massif Figure 2; [80–82]. There, an Ordovician quartz diorite pluton dated at 495 ± 40 Ma by Rb-Sr method on whole rock, and 457 ± 10 Ma by U/Pb method on zircon [82], and more recently between 504 and 466 Ma by U-Pb method on zircon [61] now changed to orthogneiss, forms the core of an NW-SE elongated metamorphic dome successively surrounded by biotite–sillimanite–muscovite–K-feldspar, biotite–garnet–staurolite, biotite–muscovite, and biotite–chlorite micaschists from the internal to the external parts of the dome. The local occurrences of metatexites and muscovite–K-feldspar micaschists and gneiss comply with HT/MP conditions developed during a crustal melting stage. Muscovite from the Plouguenast orthogneiss yields $^{40}Ar/^{39}Ar$ age at 339 ± 1 Ma, and a limited plateau at 350 Ma interpreted as an indicator of an early HT doming stage, but a pre-doming event cannot be ruled out [83,84]. Furthermore, kyanite and staurolite porphyroblasts are found either as porphyroblasts in biotite–garnet micaschists or as inclusions in andalusite porphyroblasts ascribed to contact metamorphism developed around two-mica plutons. This assemblage argues for an MP/MT metamorphic event that predated the HT/MP one. According to Saunier [81], the thermo-barometric conditions for the early event are about 650–700 °C and 0.7–1 GPa.

In the present state of knowledge, the Pontivy–Coray, and Plouguenast areas present quite similar tectono-metamorphic features. An undated, but probably older than 350 Ma, MP/MT event with biotite, garnet, staurolite, and kyanite formed during a regional event in this western part of the CNAD. The occurrence of kyanite can be interpreted as the relict of an early (M0) prograde stage (or increment) of the same main syn-metamorphic deformation (D1/M1). It was followed by an MP/HT (D2/M2) event with muscovite–sillimanite–K-feldspar developed in migmatitic domes. Lastly, a late HT/LP (M3) event, which occurred at ca. 315 Ma, is related to the contact metamorphic aureole of the Late Carboniferous plutons. A Late Devonian–Early Carboniferous age, although not documented in the Plouguenast dome, but recorded in the Pontivy–Coray area is assumed here for the regional events M0 and D1-M1 (Table 3). In order to account for the formation of kyanite porphyroblasts, we argue that a blind thrust would be responsible for the burial of

a part of the Neoproterozoic formations that reached relatively high-pressure conditions (ca 1 GPa, and 600–700 °C) during the M0 event. The rocks involved in the thrust-related thickening D0-D1 event experienced an isothermal P decrease, responsible for the development of MP/HT conditions and crustal melting during M2. The bulk architecture of Central Brittany is depicted in a synthetic crustal-scale cross-section (Figure 13; see location in Figure 2). The kinematic aspects of the D1/M1 event will be discussed at the wider scale of the Armorican and Massif Central Variscan framework (see Section 5.3).

Table 3. Synthesis of the tectono-metamorphic events recognized in the Pontivy–Coray area and extrapolated to the Plouguenast area.

Event	Metamorphism	P-T Conditions	Structure and Tectonics	Age
M0 early stage of M1	Kyanite, and aligned inclusions in porphyroblasts	0.9–1 GPa, 500–650 °C	Not documented Intracrustal thrusting?	360–355?
D1/M1	MP/MT Biotite–staurolite–garnet	0.8–0.6 GPa, 500 °C	Regional foliation NW-SE stretching lineation Top-to-the NW shearing Intracrustal thrusting?	360–355 Ma
D2/M2	MP/HT Sillimanite–K-feldspar muscovite	0.6–0.5 GPa, 700–750 °C	Top-to-the NE shearing (local) NE-SW crenulation lineation Doming	355–347 Ma
M3	LP/HT Garnet–andalusite Hornfels	0.25 GPa, 700 °C	Not investigated here Pluton emplacement	315 Ma

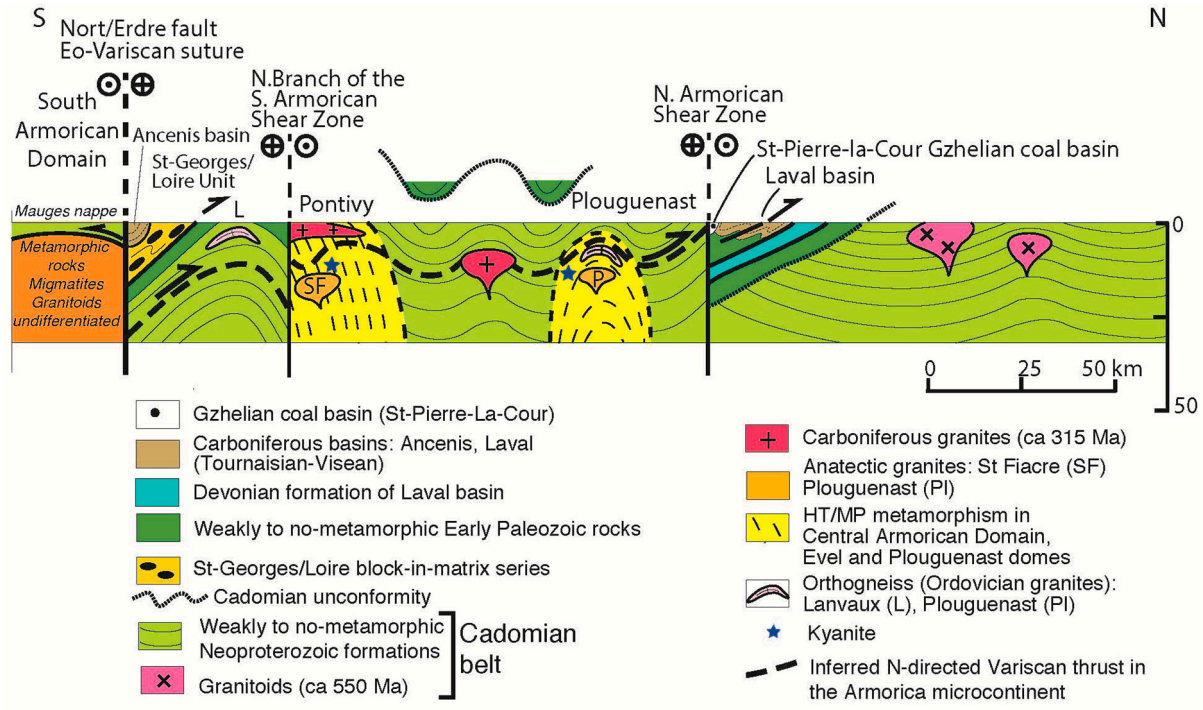

Figure 13. Interpretative crustal-scale cross-section of Central Brittany with emphasis on the Late Devonian N-directed thrusting coeval with kyanite crystallization and subsequent HT metamorphism and crustal melting.

5.3. Late Devonian–Early Carboniferous Evolution of the CNAD

In the CNAD, the absence of Famennian formations was interpreted as evidence for a tectonic event called the "Bretonian phase" Figure 3; [36,39,47,48,50,52,53,57,85–91].

However, the nature of this event remains controversial. Some authors argued for folding and thrusting, particularly well developed in the western CNAD, around Brest [54,55,87,92–95], whereas others put forward vertical, (or epeirogenic), movements with no or limited tectonic imprint [39,48,50,53,86].

From the sedimentological point of view, syn-sedimentary sliding and intraformational conglomerates are recorded in the Frasnian-Famennian (ca 380–360 Ma) deposits [47,49,50,87,96]. The major sedimentary break occurred at the Famennian–Tournaisian boundary (360–355 Ma). At that time, emersion and erosion of the Late and Middle Devonian formations developed in the Central-North Armorican Domain. In the Laval, Menez-Belair, and Châteaulin areas, the amount of erosion was estimated at about 1000–1500 m, and Late Devonian pebbles are found in those basins [48]. Tournaisian deposits are represented by terrigenous and volcanic rocks with coarse-grained sandstone, pebbly mudstone, and olistoliths, indicating a tectonic instability controlled by vertical movements with possibly a transcurrent component [48,97,98].

These epeirogenic movements were coeval with a bimodal magmatism. A dolerite dyke swarm is widespread in the north part of the CNAD [99–101]. N. of Laval basin, microgabbros yield apatite LA-ICP-MS ages around 370–360 Ma [102]. Recently, a study of the Hf isotopic composition of Famennian detrital zircon recovered in the Tournaisian sandstone of the Laval basin documented a mantle source contribution in the genesis of that Famennian mafic magmatism [103]. The syn-tectonic metamorphism in the Pontivy–Coray and Plouguenast areas can also be ascribed to the Late Devonian–Tournaisian Bretonian phase. The magmatic, metamorphic, and structural features recognized in the Central North Armorican Domain are presented in a synoptic chart (Figure 14).

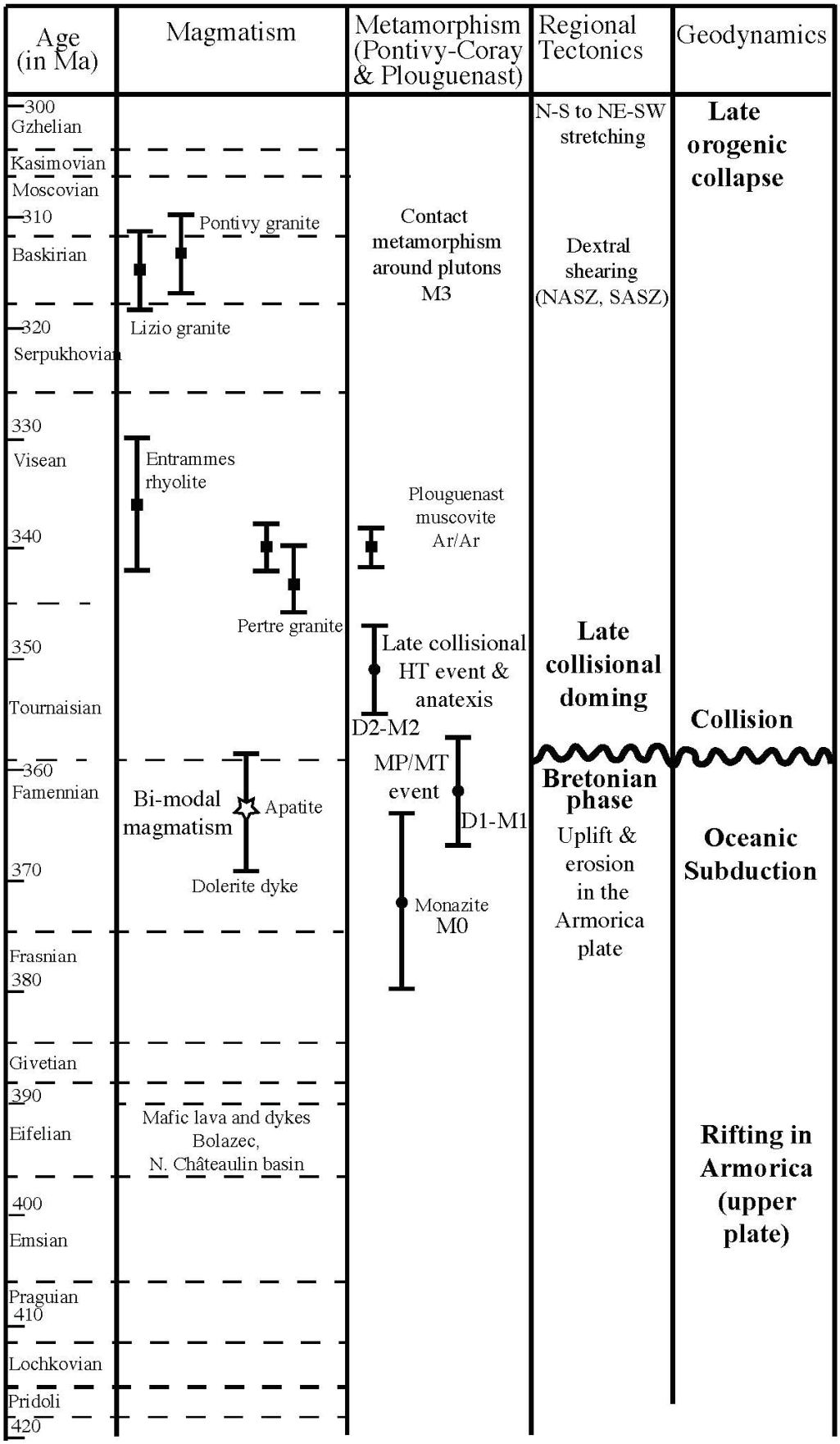

Figure 14. Synoptic chart of the metamorphic, magmatic, and tectonic events experienced in Armorica with radiometric ages provided in [59,60,78,82,102,104].

5.4. A Possible Late Devonian–Early Carboniferous Geodynamic Model for Armorica

In this section, a geodynamic scenario that integrates both the structural and metamorphic features developed in the middle crust in the Pontivy–Coray and Plouguenast areas and the sedimentary ones recognized in the upper crust of the CNAD is discussed (Figure 15). The model discussed here is restricted to the Late Devonian–Early Carboniferous evolution of Armorica and northern domains. The eo-Variscan events that developed between the Southern and Central North Armorican domains are not considered here for details, see [18,45] and enclosed references.

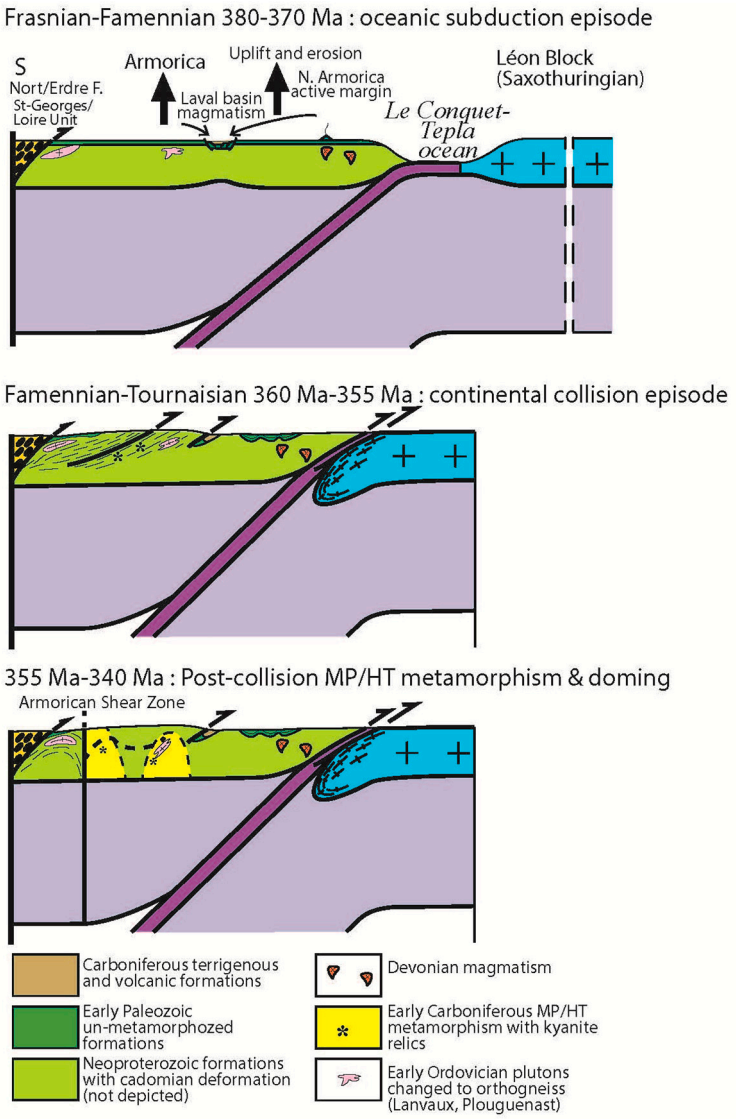

Figure 15. A possible geodynamic evolution model of the two Bretonian episodes in Armorica from Late Devonian (ca 370) to Middle Carboniferous (ca 340 Ma). The eo-Variscan (Siluro-Devonian), and late Variscan (Late Carboniferous) events are not depicted.

During the Late Devonian, the Armorica microcontinent belonged to the upper plate of a convergent system represented by the closure of the Le Conquet-Tepla ocean accommodated by a southward subduction that was responsible for the erosion of the Late to Middle formations, except in some restricted areas, such as S. of Brest, where these series have been trapped into grabens [93]. At that time, the Châteaulin, Menez-Belair, and Laval basins might have started to open as pull-apart basins along the NASZ, e.g., [42,55,90,95,96,98]. It is worth noting that although often proposed, at that time, the dextral sense of shear

was not supported by any structural data. A subduction-related calc-alkaline Devonian magmatism is not documented in Armorica either, but the bimodal magmatism recognized in the CNAD is generally correlated to this subduction [17,101,103].

The oceanic subduction of Le Conquet-Tepla ocean was followed by the continental collision of Armorica with the Léon block, a part of the Saxo-Thuringian microcontinent, at 360–355 Ma. In the middle crust of Armorica, the Neoproterozoic formations were ductilely deformed and metamorphosed under MP/MT conditions. Kyanite, garnet, and staurolite assemblages developed in the footwall of low-angle thrusts. The NW-SE mineral and stretching lineation with a top-to-the-NW shearing is ascribed to this collisional stage. In map view, the shearing direction is oblique to the present structural grain of the Armorican Massif. However, it must be taken into account that this pattern does not represent the primary Early Carboniferous geometry that has been disturbed by the Late Carboniferous dextral strike-slip shearing.

Around 355–340 Ma, a late- to post-collisional thermal event gave rise to the formation of HT domes in the CNAD. The final and most obvious tectono-magmatic event in the Armorican Massif was the dextral ductile shearing and syn-kinematic plutonism along the NASZ, N., and S. branches of the SASZ. A ca 40 km offset was estimated along the North Branch of the SASZ [62]. The same value, at least, can be taken for the other Armorican shear zones; thus, a 150 to 200 km would have to be considered for a paleogeodynamic reconstruction of the Armorica microcontinent, however, such a reconstruction is beyond the scope of this paper, see [83]. Therefore, these late structures are not considered in Figure 15, which deals only with the Late Devonian–Early Carboniferous evolution.

In the proposed geodynamic scenario, it is worth emphasizing that the "Bretonian phase" has a dualistic significance. In order to clarify the geodynamic evolution of the Armorican Massif, it would be more rigorous to distinguish two episodes, namely: (i) a pre-Late Famennian (older than 365 Ma) sub-phase corresponding to the uplift, erosion, and magmatism of Armorica in response to the southward subduction of the Le Conquet-Tepla ocean; and (ii) a Late Famennian–Tournaisian (360–345 Ma) sub-phase corresponding to the continental collision between Armorica and Saxo-Thuringia.

At the scale of the French Variscan massifs, the NW-SE-directed sinistral shearing is also recognized in the Lanvaux and St-Georges-sur-Loire units [44,105–107]; Figure 1. In the South Armorican Domain, particularly in Vendée, top-to-the-W or NW ductile shearing is coeval with an MP/MT metamorphism [108–111]. A similar pattern is also described in many places in the French Massif Central, e.g., [17,45,91,112–115]. This widespread structure, ascribed to the D2 event [17,104,115], is interpreted as the consequence of the collision between the Gondwana + Armorica block and the Léon (or Saxo-Thuringian) microcontinent [91,103]. In this view, the top-to-the NW ductile shearing described here in the Pontivy–Coray area appears as relevant to the same D2 event.

6. Conclusions

The structural and metamorphic features described here in the Pontivy–Coray area of the CNAD, allow us to draw the following conclusions.

(1) In spite of its tectonic position in the upper plate during the Variscan orogeny, the Armorica microcontinent did not behave as a rigid block but experienced several syn-metamorphic tectonic events during its collision with the Saxo-Thuringian (or Léon) block.

(2) From the metamorphic point of view, the study area successively underwent an MP/MT and then an MP/HT stage in the Famennian–Tournaisian. The first one is associated with a top-to-the-NW ductile shearing, coeval with the collision.

(3) These new insights allow us to clarify the geodynamic meaning of the "Bretonian phase" in the CNAD, which can be subdivided into two episodes.
   (i) An early episode that occurred before the Late Famennian (older than 360 Ma), corresponds to the uplift and erosion of the Armorica microcontinent in relation to the southward subduction of the Le Conquet-Tepla ocean below Armorica.
   (ii) A late one during the Famennian–Tournaisian, related to the continental collision.

(4) The late- to post-orogenic tectono-metamorphic events were accommodated by transpressional tectonics represented at depth by the dextral shearing along the SASZ and the NASZ coeval with syn-emplacement plutons and in the upper crust by the folding and thrusting of the Tournaisian–Visean basins.

Author Contributions: All authors contributed to conceptualization and writing. All authors have read and agreed to the published version of the manuscript.

Funding: This research was funded by ISTO through the Labex Voltaire grant. The APC was granted by the Journal.

Data Availability Statement: Detail of data processing is available upon request.

Acknowledgments: Field and laboratory expenses have been founded by Labex Voltaire. S. Janiec, P. Juillot, and I. Di Carlo are acknowledged for preparing thin sections, operating SEM, and microprobe at ISTO. The Editor and the anonymous reviewers are thanked for their constructive comments that helped us to improve the article.

Conflicts of Interest: The authors declare no conflict of interest.

References

1. Mattauer, M. Sur le mécanisme de formation de la schisstosité dans l'Himalaya. *Earth Planet. Sci. Lett.* **1975**, *28*, 144–154. [CrossRef]
2. Brunel, M. Ductile thrusting in the Himalayas: Shear sense criteria and stretching lineations. *Tectonics* **1986**, *5*, 247–265. [CrossRef]
3. Haines, S.; Klemperer, S.; Brown, L.; Guo, J.; Mechie, J.; Meissner, R.; Ross, A.; Zhao, W. INDEPTH III seismic data: From surface observations to deep crustal processes in Tibet. *Tectonics* **2003**, *22*, 1–8. [CrossRef]
4. Le Fort, P. Himalayas: The collided rang. Present knowledgeof the continental arc. *Am. J. Sci.* **1975**, *275*, 1–44.
5. Yin, A. Cenozoic tectonic evolution of the Himalayan orogen as constrained by along-strike variation of structural geometry, exhumation history, and foreland sedimentation. *Earth Sci. Rev.* **2006**, *76*, 1–131. [CrossRef]
6. Xu, Z.-Q.; Dilek, Y.; Yang, J.-S.; Liang, F.-H.; Liu, F.; Ba, D.-Z.; Cai, Z.-H.; Li, G.-W.; Dong, H.-W.; Ji, S.-C. Crustal structure of the Indus–Tsangpo suture zone and its ophiolites in southern Tibet. *Gondwana Res.* **2015**, *27*, 507–524. [CrossRef]
7. Metcalf, K.; Kapp, P. The Yarlung suture mélange, Lopu Range, southern Tibet: Provenance of sandstone blocks and transition from oceanic subduction to continental collision. *Gondwana Res.* **2017**, *48*, 15–33. [CrossRef]
8. Roure, F.; Polino, R.; Nicolich, R. Poinçonnement, rétrocharriages et chevauchements postbasculement dans les Alpes occidentales: Évolution intracontinentale d'une chaîne de collision. *C. R. Acad. Sci. Paris* **1989**, *309*, 283–290.
9. Schmid, S.M.; Fugenschuh, B.; Kissling, E.; Schuster, R. Tectonic map and overall architecture of the Alpine orogen. *Eclogae Geol. Helv.* **2004**, *97*, 93–117. [CrossRef]
10. Lemoine, M.; Graciansky, P.-C.; Tricart, P. *De L'océan à la Chaîne de Montagnes. Tectonique Des Plaques Dans Les Alpes*; Gordon and Breach Publishers: Paris, France, 2000.
11. Agard, P.; Lemoine, M. *Faces of the Alps: Structure and Geodynamic Evolution*; Commission for the Geological Map of the World: Paris, France, 2005.
12. Bonnet, G.; Chopin, C.; Locatelli, M.; Kylander-Clark, A.; Hacker, B. Protracted subduction of the European hyperextended margin revealed by rutile U-Pb geochronology across the Dora-Maira Massif (western Alps). *Tectonics* **2022**, *41*, TC007170. [CrossRef]
13. Dewey, J.F.; Burke, K.C.A. Tibetan, Variscan and Precambrian basement reactivation: Products of continental collision. *J. Geol.* **1973**, *81*, 683. [CrossRef]
14. Matte, P. La chaîne Varisque parmi les chaînes Paléozoïques périatlantiques, modèle d'évolution et position des grands blocs continentaux au Permo-Carbonifère. *Bull. Soc. Géol. Fr.* **1986**, *2*, 9–24. [CrossRef]

15. Matte, P. The Variscan collage and orogeny (480–290 Ma) and the tectonic definition of the Armorica microplate: A review. *Terra Nova* **2001**, *13*, 122–128. [CrossRef]
16. Carosi, R.; Palmeri, R. Orogen-parallel tectonic transport in the Variscan belt of northeastern Sardinia (Italy): Implications for the exhumation of medium-pressure metamorphic rocks. *Geol. Mag.* **2002**, *139*, 497–511. [CrossRef]
17. Faure, M.; Bé Mézème, E.; Duguet, M.; Cartier, C.; Talbot, J.Y. Paleozoic tectonic evolution of medio-europa from the example of the French Massif Central and Massif Armoricain. *J. Virtual Explor.* **2005**, *19*, 1–25. [CrossRef]
18. Ballèvre, M.; Bosse, V.; Ducassou, C.; Pitra, P. Palaeozoic history of the Armorican Massif: Models for the tectonic evolution of the suture zones. *C. R. Geosci.* **2009**, *341*, 174–201. [CrossRef]
19. Martínez Catalán, J.R.; Arenas, R.; Abati, J.; Sánchez Martínez, S.; Díaz García, F.; Fernández Suárez, J.; González Cuadra, P.; Castiñeiras, P.; Gómez Barreiro, J.; Díez Montes, A.; et al. A rootless suture and the loss of the roots of a mountain chain: The Variscan belt of NW Iberia. *C. R. Geosci.* **2009**, *341*, 114–126. [CrossRef]
20. Murphy, B.; Cousens, B.; Braid, J.; Strachan, R.; Dostal, J.; Keppie, D.; Nance, D. Highly depleted oceanic lithosphere in the Rheic Ocean: Implications for Paleozoic plate reconstructions. *Lithos* **2011**, *123*, 165–175. [CrossRef]
21. Lardeaux, J.-M.; Schulmann, K.; Faure, M.; Janousek, V.; Lexa, O.; Skrzypek, E.; Edel, J.-B.; Stipska, P. The Moldanubian Zone in French Massif Central, Vosges/Schwarzwald and Bohemian Massif revisited: Differences and similarities. *Geol. Soc. Lond. Spec. Publ.* **2014**, *405*, 7–44. [CrossRef]
22. Pereira, M.; Gutíerrez-Alonso, G.; Murphy, J.; Drost, K.; Gama, C.; Silva, J. Birth and demise of the Rheic Ocean magmatic arc(s): Combined U–Pb and Hf isotope analyses in detrital zircon from SW Iberia siliciclastic strata. *Lithos* **2017**, *278–281*, 383–399. [CrossRef]
23. Edel, J.B.; Schulmann, K.; Lexa, O.; Lardeaux, J.-M. Late Palaeozoic palaeomagnetic and tectonic constraints for amalgamation of Pangea supercontinent in the European Variscan belt. *Earth-Sci. Rev.* **2018**, *177*, 589–612. [CrossRef]
24. Alvaro, J.; Casas, J.-M.; Quesada, C. Reconstructing the pre-Variscan puzzle of Cambro-Ordovician basement rocks in the southwestern European margin of Gondwana. *Geol. Soc. Lond. Spec. Publ.* **2020**, *503*, 531–562. [CrossRef]
25. Neubauer, F.; Frisch, W. The Austroalpine metamorphic basement east of the Tauern Window. In *The Pre-Mesozoic Geology in the Alps*; von Raumer, J., Neubauer, F., Eds.; Springer: Berlin/Heidelberg, Germany, 1993; pp. 515–536.
26. von Raumer, J.F. Pre-Mesozoic Alpine basements—Their place in the European Paleozoic framework. *GSA Bull.* **2013**, *125*, 89–108. [CrossRef]
27. Faure, M.; Ferrière, J. Reconstructing the Variscan Terranes in the Alpine basement: Facts and arguments for an alpidic orocline. *Geosciences* **2022**, *12*, 65. [CrossRef]
28. Lorenz, V. Formation of Hercynian subplates, possible causes and consequences. *Nature* **1976**, *262*, 374–376. [CrossRef]
29. Badham, J.P.N. Strike-slip orogens—An explanation for the Hercynides. *J. Geol. Soc.* **1982**, *139*, 493–504. [CrossRef]
30. Perroud, H.; Van der Voo, R.; Bonhommet, N. Paleozoic evolution of the Armorica plate on the basis of the paleomagnetic data. *Geology* **1984**, *12*, 579–582. [CrossRef]
31. Van der Voo, R. Pre-Mesozoic paleomagnetism and plate tectonics. *Annu. Rev. Earth Planet. Sci.* **1982**, *10*, 191–220.
32. Robardet, M. The Armorica microplate: Fact or fiction? Critical review of the concept and contradictory palaeobiogeographical data. *Palaeogeogr. Palaeoclimatol. Palaeoecol.* **2003**, *195*, 125–148. [CrossRef]
33. Le Corre, C.; Le Théoff, B. Zonéographie de la déformatiion finie, de la fabrique et du métamorphisme dans un segment de la chaîne hercynienne armoricaine. *Bull. Soc. Géol. Fr.* **1976**, *18*, 1435–1442. [CrossRef]
34. Gapais, D.; Le Corre, C. Is the hercynian belt of Brittany a major shear zone? *Nature* **1980**, *288*, 574–576. [CrossRef]
35. Hanmer, S.K.; Le Corre, C.; Berthé, D. The role of Hercynian granites in the deformation and metamorphism of Brioverian and Palaeozoic rocks of Central Brittany. *J. Geol. Soc. Lond.* **1982**, *139*, 85–93. [CrossRef]
36. Barrière, M.; Rolet, J.; Thonon, P. Le magmatisme, marqueur de l'évolution orogénique, en domaine hercynien Ouest-Armoricain. *C. R. Acad. Sci. Paris* **1983**, *296*, 917–922.
37. Le Corre, C.; Auvray, B.; Ballèvre, M.; Robardet, M. Le Massif Armoricain. *Sci. Geol. Bull.* **1991**, *44*, 31–103. [CrossRef]
38. Barrois, C. Note sur les gisements de staurotide de Bretagne. *Ann. Soc. Géol. Nord.* **1934**, *59*, 29–65.
39. Cogné, J. *Schistes Cristallins et Granites en Bretagne Méridionale. Le Domaine de l'anticlinal de Cornouailles*; Mémoire Explicatif de la carte géologique de France; Imprimerie Nationale: Paris, France, 1960; 382p.
40. Berthé, D.; Choukroune, P.; Jégouzo, P. Orthogneiss, mylonite and non-coaxial deformation of granites: The example of the South Armorican Shear Zone. *J. Struct. Geol.* **1979**, *1*, 31–42. [CrossRef]
41. Jégouzo, P. The South-Armorican Shear Zone. *J. Struc. Geol.* **1980**, *2*, 39–47. [CrossRef]
42. Rolet, J.; Le Gall, B.; Darboux, J.-R.; Thonon, P.; Gravelle, M. L'évolution géodynamique dévono-carbonifère de l'extrémité occidentale de la chaîne hercynienne d'Europe sur le transect Armorique–Cornwall. *Bull. Soc. Geol. Fr.* **1986**, *2*, 43–54. [CrossRef]
43. Faure, M.; Sommers, C.; Melleton, J.; Cocherie, A.; Lautout, O. The Léon domain (French Massif Armoricain): A westward extension of the mid-German crystalline rise? Structural and geochronological insights. *Int. J. Earth Sci.* **2009**, *99*, 65–81. [CrossRef]

44. Cartier, C.; Faure, M. Structure and geodynamic evolution of the Gondwana–Armorica boundary in the Ligerian domain (Armorican Massif, France). *Int. J. Earth Sci.* **2004**, *93*, 945–958. [CrossRef]
45. Faure, M.; Bé Mézème, E.; Cocherie, A.; Rossi, P.; Chemenda, A.; Boutelier, D. Devonian geodynamic evolution of the Variscan Belt, insights from the French Massif Central and Massif Armoricain. *Tectonics* **2008**, *27*, TC2008. [CrossRef]
46. Cogné, J. Le Massif Armoricain. In *Géologie de la France*; Debelmas, J., Ed.; Doin: Paris, France, 1974; pp. 105–161.
47. Lardeux, H.; Chauvel, J.J.; Henry, J.L.; Morzadec, P.; Paris, F.; Racheboeuf, P.; Robardet, M. Evolution géologique du Massif Armoricain au cours des temps ordoviciens, siluriens, et dévoniens. *Chaîne Varisque D'Eur. Moy. Occident.* **1977**, *243*, 181–192.
48. Paris, F.; Morzadec, P.; Le Hérissé, A.; Pelhate, A. Late Devonian—Early Carboniferous events in the Armorican Massif (Western France): A review. *Ann. Soc. Géol. Belg.* **1986**, *109*, 187–195.
49. Morzadec, P.; Paris, F.; Plusquellec, Y.; Racheboeuf, P.; Weyant, M. Devonian stratigraphy and paleogeography of the Armorican Massif (Western France). In *Devonian of the World: Proceedings of the 2nd International Symposium on the Devonian System, Calgary, AB, 1987, Canada*; McMillan, N.J., Embry, A.F., Glass, D.J., Eds.; Canadian Society of Petroleum Geologists: Ottawa, ON, Canada, 1988; Volume 14, pp. 401–420.
50. Robardet, M.; Bonjour, J.-L.; Paris, F.; Morzadec, P.; Racheboeuf, P.R. Ordovician, Silurian, and Devonian of the Medio-North Armorican Domain. In *Pre-Mesozoic Geology in France and Related Areas*; Keppie, J.D., Ed.; Springer: Berlin/Heidelberg, Germany, 1994; pp. 142–151.
51. Chantraine, J.; Egal, E.; Thiéblement, D.; Le Goff, E.; Guerrot, C.; Ballèvre, M.; Guennoc, P. The Cadomian active margin (North Armorican Massif, France): A segment of the North Atlantic Panafrican belt. *Tectonophysics* **2001**, *331*, 1–18. [CrossRef]
52. Pelhâte, A. Le Carbonifère inférieur du bassin de Laval, Massif Armoricain. *Mém. Soc. Géol. Minéral. Bretagne* **1971**, *5*, 315.
53. Paris, F.; Le Hérissé, A.; Pelhâte, A.; Weyant, M. Les formations carbonifères et la phase bretonne dans le synclinorium du Ménez-Bélair: Essai de synthèse. *Bull. Soc. Géol. Minéral. Bretagne* **1982**, *14*, 19–33.
54. Darboux, J.R. Caractérisation du régime cisaillant de la déformation hercynienne dans les Monts d'Arrée (Massif Armoricain, France). *C. R. Acad. Sci. Paris* **1981**, *292*, 1497–1500.
55. Rolet, J.; Gresselin, F.; Jégouzo, P.; Ledru, P.; Wyns, R. Intracontinental Hercynian events in the Armorican Massif. In *Pre-Mesozoic Geology of France and Related Areas*; Keppie, J.D., Ed.; Springer: Berlin, Germany, 1994; pp. 195–219.
56. Gresselin, F. Evolution Structurale D'une Transvealedu Socle Casomo-Varisque du Nord-Est de l'Armorique. Insertion Dans un Profil Ouest Européen. Ph.D. Thesis, Université de Caen, Caen, France, 1990.
57. Le Gall, B.; Loboziak, S.; Le Hérissé, A. Le flanc sud du synclinorium carbonifère de Châteaulin (Massif Armoricain, France): Une bordure de bassin réactivée en contexte décro-chevauchant. *Bull. Soc. Géol. Fr.* **1992**, *163*, 13–26.
58. Capdevila, R. Les granites varisques du Massif Armoricain. *Bull. Soc Géol. Minéral. Bretagne* **2010**, *7*, 1–52.
59. Tartèse, R.; Poujol, M.; Ruffet, G.; Boulvais, P.; Yamato, P.; Košler, J. New U-Pb zircon and $^{40}Ar/^{39}Ar$ muscovite age constraints on the emplacement of the Lizio syn-tectonic granite (Armorican Massif, France). *C. R. Geosci.* **2011**, *343*, 443–453. [CrossRef]
60. Ballouard, C.; Poujol, M.; Boulvais, P.; Zeh, A. Crustal recycling and juvenile addition during lithospheric wrenching: The Pontivy-Rostrenen magmatic complex, Armorican Massif (France), Variscan belt. *Gondwana Res.* **2017**, *49*, 222–247. [CrossRef]
61. Ballouard, C.; Poujol, M.; Zeh, A. Multiple crust reworking in the French Armorican Variscan belt: Implication for the genesis of uranium-fertile leucogranites. *Int. J. Earth Sci.* **2018**, *107*, 2317–2336. [CrossRef]
62. Jégouzo, P.; Rossello, A.E. La branche nord du cisaillement Sud-Armoricain: Un essai d'évaluation du déplacement par l'analyse des mylonites. *C. R. Acad. Sci. Paris* **1988**, *307*, 1825–1831.
63. Schulz, B.; Audren, C.; Triboulet, C. Regional vs contact metamorphism of garnet metapelites in the vicinity of Late Variscan granites (Central Armorican Domain, Brittany, France). *Geol. Rundsch.* **1998**, *87*, 78–93. [CrossRef]
64. Schulz, B. Monazite EPM-Th-U-Pb age pattern in Variscan metamorphic units in the Armorican Massif (Brittany, France). *Z. Der Dtsch. Ges. Für Geowiss.* **2013**, *164*, 13–335.
65. Barrière, M.; Chauris, L.; Le Bail, F. Nodules de silicates d'alumine autour de granites en Bretagne méridionale. *Bull. Soc. Fr. Minéral. Cristallogr.* **1973**, *96*, 150–154.
66. Suzuki, K.; Adachi, M. Precambrian provenance and Silurian metamorphism of the Tsubonosawa paragneiss in the South Kitakami terrane, Northeast Japan, revealed by the chemical Th–U–total Pb isochron ages of monazite, zircon and xenotime. *Geochem. J.* **1991**, *25*, 357–376. [CrossRef]
67. Zhu, X.K.; O'Nions, R.K. Zonation of monazite in metamorphic rocks and its implications for high temperature thermochronology: A case study from the Lewisian terrain. *Earth Planet. Sci. Lett.* **1999**, *171*, 209–220. [CrossRef]
68. Cocherie, A.; Legendre, O.; Peucat, J.J.; Kouamelan, A.N. Geochronology of polygenetic monazites constained by in situ electron microprobe Th–U–total Pb determination: Implications for lead behaviour in monazite. *Geochim. Cosmochim. Acta* **1998**, *62*, 2475–2497. [CrossRef]
69. Parrish, R. U–Pb dating of monazite and its application to geological problems. *Can. J. Earth Sci.* **1990**, *27*, 1431–1450. [CrossRef]
70. Cocherie, A.; Bé Mézème, E.; Legendre, O.; Fanning, M.; Faure, M.; Rossi, P. Electron microprobe dating as a tool for understanding closure of U–Th–Pb system in monazite from migmatite. *Am. Mineral.* **2005**, *90*, 607–618. [CrossRef]

71. Bé Mézème, E.; Cocherie, A.; Faure, M.; Legendre, O.; Rossi, P. Electron microprobe monazite geochronology: A tool for evaluating magmatic age domains. Examples from the Variscan French Massif Central. *Lithos* **2006**, *87*, 276–288. [CrossRef]
72. Faure, M.; Cocherie, A.; Bé-Mézème, E.; Charles, N.; Rossi, P. Middle Carboniferous crustal melting in the Variscan Belt: New insights from U–Th–Pbtot. monazite and U–Pb zircon ages of the Montagne Noire Axial Zone (southern French Massif Central). *Gondwana Res.* **2010**, *18*, 653–673. [CrossRef]
73. Faure, M.; Cocherie, A.; Gaché, J.; Esnault, C.; Guerrot, C.; Rossi, P.; Lin, W.; Li, Q. Middle Carboniferous intracontinental subduction in the Outer Zone of the Variscan belt (Montagne Noire Axial Zone, French Massif Central): Multimethod geochronological approach of polyphase metamorphism. *Geol. Soc. Lond. Spec. Publ.* **2014**, *405*, 289–311. [CrossRef]
74. Do Couto, D.; Faure, M.; Augier, R.; Cocherie, A.; Rossi, P.; Li, X.H.; Lin, W. Monazite U–Th–Pb EPMA and zircon U–Pb SIMS chronological constraints on the tectonic, metamorphic, and thermal events in the inner part of the Variscan orogen, example from the Sioule series, French Massif Central. *Int. J. Earth Sci.* **2016**, *105*, 557–579. [CrossRef]
75. Gasquet, D.; Bertrand, J.-M.; Paquette, J.-L.; Lehmann, J.; Ratzov, G.; De Ascenção Guedes, R.; Tiepolo, M.; Boullier, A.M.; Scaillet, S.; Nomade, S. Miocene to Messinian deformation and hydrothermalism in the Lauzière Massif (French Western Alps): New U–Th–Pb and Argon ages. *Bull. Soc. Géol. Fr.* **2010**, *181*, 227–241. [CrossRef]
76. Paquette, J.-L.; Tiepolo, M. High resolution (5 µm) U–Th–Pb isotopes dating of monazite with excimer laser ablation (ELA)-ICPMS. *Chem. Geol.* **2007**, *240*, 222–237. [CrossRef]
77. Paton, C.; Woodhead, J.D.; Hellstrom, J.C.; Herg, J.M.; Greig, A.; Maas, R. Improved laser ablation U-Pb zircon geochronology through robust downhole fractionation correction. *Geochem. Geophys. Geosystems* **2010**, *11*, 3. [CrossRef]
78. Poujol, M.; Pitra, P.; Van Den Driessche, J.; Tartèse, R.; Ruffet, G.; Paquette, J.-L.; Poilvet, J.-C. Two-stage partial melting during the Variscan extensional tectonics (Montagne Noire, France). *Int. J. Earth Sci.* **2017**, *106*, 477–500. [CrossRef]
79. Stacey, J.S.; Kramer, J.D. Approximation of terrestrial lead isotope evolution by a two stage model. *Earth Planet. Sci. Lett.* **1975**, *26*, 207–221. [CrossRef]
80. Chantraine, J.; Carric, G.; Dadet, P.; Flageollet, J.-C.; Sagon, J.-P.; Talbo, H.; Mulot, B. *Notice Explicative, Carte Géol. France (1/50,000), Feuille Moncontour (279)*; BRGM: Orléans, France, 1979; 43p.
81. Saunier, J.-F. Un domaine cristallophyllien dans le Protérozoïque supérieur (briovérien) de Bretagne centrale: Le dôme de Plouguenast (Côtes du Nord). *Doc. BRGM* **1986**, *109*, 125p.
82. Thomas, E.; Sevin, B.; Lesimple, S.; Le Berre, P.; Fullgraf, T.; Beuchet, L.; Carn, A. *Notice Explicative, Carte Géol. France (1/50,000), Feuille Loudéac (314)*; BRGM: Orléans, France, 2010; 112p.
83. Gumiaux, C. Modélisation du Cisaillement Hercynien de Bretagne Centrale: Déformation Crustale et Implications Lithosphériques. Ph.D. Thesis, University of Rennes, Rennes, France, 2003; 265p.
84. Gumiaux, C.D.; Gapais, J.-P.; Brun, J.; Chantraine, G. Ruffet, Tectonic history of the Hercynian Armorican Shear belt (Brittany, France). *Geodin. Acta* **2004**, *17*, 289–307. [CrossRef]
85. Stille, H. Zur Einführung in die Phasen des paläozoischen Gebirgsbildung. *Z. Der Dtsch. Geol. Ges.* **1928**, *80*, 1–25.
86. Cogné, J. Observations sur l'âge et la signification de la phase bretonne. *C. R. Sess. Extraordin. Bull. Soc. Belg. Géol. Paléontol. Hydrogéol.* **1965**, *73*, 239–243.
87. Babin, C.; Darboux, J.-R.; Duée, G.; Gravelle, M.; Morzadec, P.; Plusquellec, Y.; Thonon, P. Tectoniques tangentielles et tectoniques superposées dans le Dévonien de la rade de Brest (N. Finistère). *C. R. Acad. Sci. Paris* **1975**, *280*, 259–262.
88. Plaine, J. La Bordure Sud Du Synclinorium Paléozoïque de Laval (Massif Armoricain): Stratigraphie, Volcanisme, Structure. Ph.D. Thesis, Université de Rennes, Rennes, France, 1976; 212p.
89. Regnault, S. Stratigraphie et structure du Paléozoïque dans le Ménez-Bélair occidental (synclinorium médian armoricain). *Bull. Soc. Géol. Minéral. Bretagne* **1981**, *13*, 111.
90. Rolet, J. La phase bretonne en Bretagne. *Bull. Soc. Géol. Miner. Bretagne* **1982**, *14*, 63–71.
91. Faure, M.; Li, X.H.; Lin, W. The northwest-directed "Bretonian phase" in the French Variscan Belt (Massif Central and Massif Armoricain): A consequence of the Early Carboniferous Gondwana–Laurussia collision. *C. R. Geosci.* **2017**, *349*, 126–136. [CrossRef]
92. Darboux, J.-R.; Gravelle, M.; Pelhâte, A.; Rolet, J. L'évolution tectonique de la terminaison occidentale du domaine centre-armoricain au Dévonien et au Carbonifère. *C. R. Acad. Sci. Paris* **1977**, *284*, 1151–1154.
93. Rolet, J.; Thonon, P. La semelle d'un charriage hercynien majeur effondrée par un réseau de fractures en régime coulissant dextre, sa mise en évidence grâce aux marqueurs filoniens de la rade de Brest (Massif Armoricain). *C. R. Acad. Sci. Paris* **1978**, *287*, 1099–1102.
94. Darboux, J.R.; Plusquellec, Y. Tectonique du Dévonien inférieur de la Presqu'île de Crozon: La coupe des Capucins en Roscanvel (Massif Armoricain, France). *C. R. Acad. Sci. Paris* **1981**, *292*, 1409–1411.
95. Rolet, J.; Plusquellec, Y.; Babin, C.; Deunff, J. Famennian regression and Strunian grabens in the Armorican massif. A key-area: Western Brittany. *Ann. Soc. Géol. Belg.* **1986**, *109*, 197–203.

96. Guillocheau, F. La sédimentation paléozoïque ouest-armoricaine. Histoire sédimentaire, relations tectonique-sédimentation. *Bull. Soc. Géol. Minéral. Bretagne* **1982**, *14*, 45–62.
97. Pelhâte, A. Carboniferous of the Armorican Massif. In *Pre-Mesozoic Geology in France and Related Areas*; Keppie, J.D., Ed.; Springer: Berlin/Heidelberg, Germany, 1994; pp. 162–168.
98. Houlgatte, E.; Le Hérissé, A.; Pelhâte, A.; Rolet, J. Evolution géodynamique du bassin Carbonifère de Laval. *Géol. Fr.* **1988**, *1*, 27–46.
99. Mary, G.; Le Gall, J. Le Dinantien basal du flanc Nord du Bassin de Laval à Argentré: Volcanites basiques et formations volcano-sédimentaires. *Hercynica* **1985**, *1*, 155–163.
100. Lahaye, Y.; Blais, S.; Auvray, B.; Ruffet, G. Le Volcanisme fissural paléozoïque du domaine nord-armoricain. *Bull. Soc. Géol. Fr.* **1995**, *166*, 601–612. [CrossRef]
101. Le Gall, J. Les dolérites et basaltes tholéiitiques varisques du domaine nord-armoricain. *Géol. Fr.* **1999**, *4*, 3–26.
102. Pochon, A.; Poujol, M.; Gloaguen, E.; Branquet, Y.; Cagnard, F.; Gumiaux, C.; Gapais, D. U-Pb LA-ICP-MS dating of apatite in mafic rocks: Evidence for a major magmatic event at the Devonian-Carboniferous boundary in the Armorican Massif (France). *Am. Mineral.* **2016**, *101*, 2430–2442. [CrossRef]
103. Lin, W.; Faure, M.; Meng, L. The uplift of Armorica and the Bretonian movements of the Variscan orogeny. New insights from detrital zircons in the early Carboniferous terrigenous rocks of the Laval basin (Armorican Massif, France). *G Cubed*, 2025; *in review*.
104. Vernhet, Y.; Plaine, J.; Trautmann, F.; Pivette, B. *Notice Explicative, Carte Géol. France (1/50,000), Feuille Cossé-le-Vivien (355)*; BRGM: Orléans, France, 2009; 222p.
105. Diot, H.; Blaise, J. Etude structurale dans le Précambrien et le Paléozoïque de la partie méridionale du domaine ligérien (SE du Massif Armoricain): Mauges, synclinal d'Ancenis et Sillon Houiller de basse Loire. *Bull. Soc. Géol. Minéral. Bretagne* **1978**, 31–50.
106. Cogné, J.P.; Choukroune, P.; Cogné, J. Cisaillements varisques superposés dans le massif de Lanvaux (Bretagne centrale). *C. R. Acad. Sci. Paris* **1983**, *296*, 773–777.
107. Faure, M.; Cartier, C. Déformations ductiles polyphasées dans l'antiforme orthogneissique de St-Clément-de-la-Place (unité de Lanvaux, Massif Armoricain). *C. R. Acad. Sci. Paris* **1988**, *326*, 795–802. [CrossRef]
108. Burg, J.-P. Tectonique tangentielle en Vendée littorale: Signification des linéations d'étirement E–W dans les porphyroïdes à foliation horizontale. *C. R. Acad. Sci. Paris* **1981**, *293*, 849–854.
109. Brun, J.-P.; Burg, J.-P. Combined thrusting and wrenching in the Ibero–Armorican arc: A corner effect during continental collision. *Earth Planet. Sci. Lett.* **1982**, *6*, 319–332. [CrossRef]
110. Cannat, M.; Bouchez, J.-L. Linéations N–S et E–W en Vendée littorale (Massif Armoricain). Episodes tangentiels successifs eo-hercyniens en France occidentale. *Bull. Soc. Géol. Fr.* **1986**, *8*, 299–310. [CrossRef]
111. Burg, J.-P.; Balé, P.; Brun, J.P.; Girardeau, J. Stretching lineation and transport direction in the Ibero-Armorican arc during the siluro-devonian collision. *Geodin. Acta* **1987**, *1*, 71–87. [CrossRef]
112. Roig, J.-Y.; Faure, M. La tectonique cisaillante polyphasée du Sud-Limousin. *Bull. Soc. Géol. Fr.* **2000**, *171*, 295–307. [CrossRef]
113. Duguet, M.; Faure, M. Successive shearing tectonics during the Hercynian collisional evolution of the southwestern French Massif Central. *Bull. Soc. Géol. Fr.* **2004**, *175*, 49–59. [CrossRef]
114. Bellot, J.-P.; Roig, J.-Y. Episodic exhumation of HP rocks inferred from structural data and P-T paths from the southwestern Massif Central (Variscan belt, France). *J. Struct. Geol.* **2007**, *29*, 1538–1557. [CrossRef]
115. Faure, M.; Lardeaux, J.-M.; Ledru, P. A review of the pre-Permian geology of the French Massif Central. *C. R. Geosci.* **2009**, *341*, 202–213. [CrossRef]